Carbon 139 (2018) 427–436

Contents lists available at ScienceDirect

Carbon

journal homepage: www.elsevier.com/locate/carbon

Scaling of binding affinities and cooperativities of surfactants on carbon nanotubes

Minsuk Park [a], Junmo Park [a], Jiyun Lee [b], Sang-Yong Ju [a, *]

[a] Department of Chemistry, Yonsei University, 50 Yonsei-ro, Seodaemun-Gu, Seoul, 03722, South Korea
[b] Department of Chemical and Biomolecular Engineering, Yonsei University, 50 Yonsei-ro, Seodaemun-Gu, Seoul, 03722, South Korea

ARTICLE INFO

Article history:
Received 21 February 2018
Received in revised form
23 June 2018
Accepted 1 July 2018
Available online 2 July 2018

ABSTRACT

High-end applications of single-walled carbon nanotube (SWNT) require detailed understanding of their binding affinity (K_d) with surfactants. Here, we quantitatively determined the comprehensive K_d and aggregation number (γ) of nine nonionic and anionic surfactants according to SWNT chirality. Photoluminescence (PL)-based titration using flavin mononucleotide (FMN)-SWNT complexes showing the largest redshifted optical transition enabled quantitative comparison of the surfactants and displayed distinct first and second regimes which correspond to partial and full replacements of FMN, respectively. Especially, the second transition exhibited sigmoidal PL change whose middle point denoted by the inverse of K_d slightly differs from critical micelle concentration of surfactant alone, depending on its functional groups. Moreover, nonionic surfactants displayed larger K_d and lower γ values than the anionic did. Specifically, K_d values between Pluronic F108 and sodium dodecyl sulfonate differ by four orders of magnitude. Such differences were rationalized in terms of the occupied volume of the micelle based on the hydrodynamic volume and γ. During the replacement, K_d and γ were affected by the degree of surfactant rearrangement induced by aging process, leading to more stable complex. Scaling the interactions between surfactant and SWNT provides useful guidelines to design novel SWNT sorting method using more than two surfactants.

1. Introduction

Despite advances over the last two decades, high-end applications of single-walled carbon nanotube (SWNT) hinge on a detailed understanding of the binding affinity (K_d) with surfactants because such applications necessitate a bulk quantity in solution [1–9]. Absorption spectroscopy is thought to be a quantitative way to determine K_d. However, because the absorption contains contributions not only from individually exfoliated SWNTs but also from its bundles [1,10–12], carbonaceous impurities [11–13], and the background originating from scattering [12,13], the absorbance itself cannot give quantitative information about K_d.

To determine K_d, quantum mechanical simulations [14–16] along with molecular mechanics calculations [14,17–20] have been employed to probe the energetic difference between the constituents and the adduct. Along these approaches, the experimental determination of K_d is required to understand the underlying thermodynamics. Recently, our group [21], along with others [22–24], has reported the K_d and related thermodynamic functions of several surfactants on SWNTs in which a flavin mononucleotide (FMN (**1**), see Fig. 1 for the chemical structure)-SWNT dispersion was utilized to induce changes in the effective dielectric constant (ε_{eff}) of the SWNT upon surfactant exchange [21,25]. In particular, titration methods using photoluminescence (PL) and absorption have been utilized to determine the K_d value according to nanotube chiralities, electronic properties, and enantiomers [21,26].

The specificity of K_d of more than two surfactants with SWNTs has been widely utilized to develop a novel sorting scheme of SWNTs. The most characterized routes for SWNT sorting include density gradient ultracentrifugation (DGU) [1–4], liquid column chromatography (LCC) [5–7], and two-phase extraction method using poly(ethylene oxide) (PEO)/dextran [8,9]. For instance, DGU method makes use of surfactant mixtures such as sodium cholate (SC (**7**) in Fig. 1)/sodium dodecyl sulfate (SDS (**9**)), LCC with stationary agarose-based Sephacryl exploits SC/SDS [7], or Triton X-405 (**4**)/sodium dodecylbenzene sulfonate (SDBS (**7**)) [27]. In this regard, the subtle difference in (co)surfactant organization on the

* Corresponding author.
E-mail address: syju@yonsei.ac.kr (S.-Y. Ju).

https://doi.org/10.1016/j.carbon.2018.07.003
0008-6223/

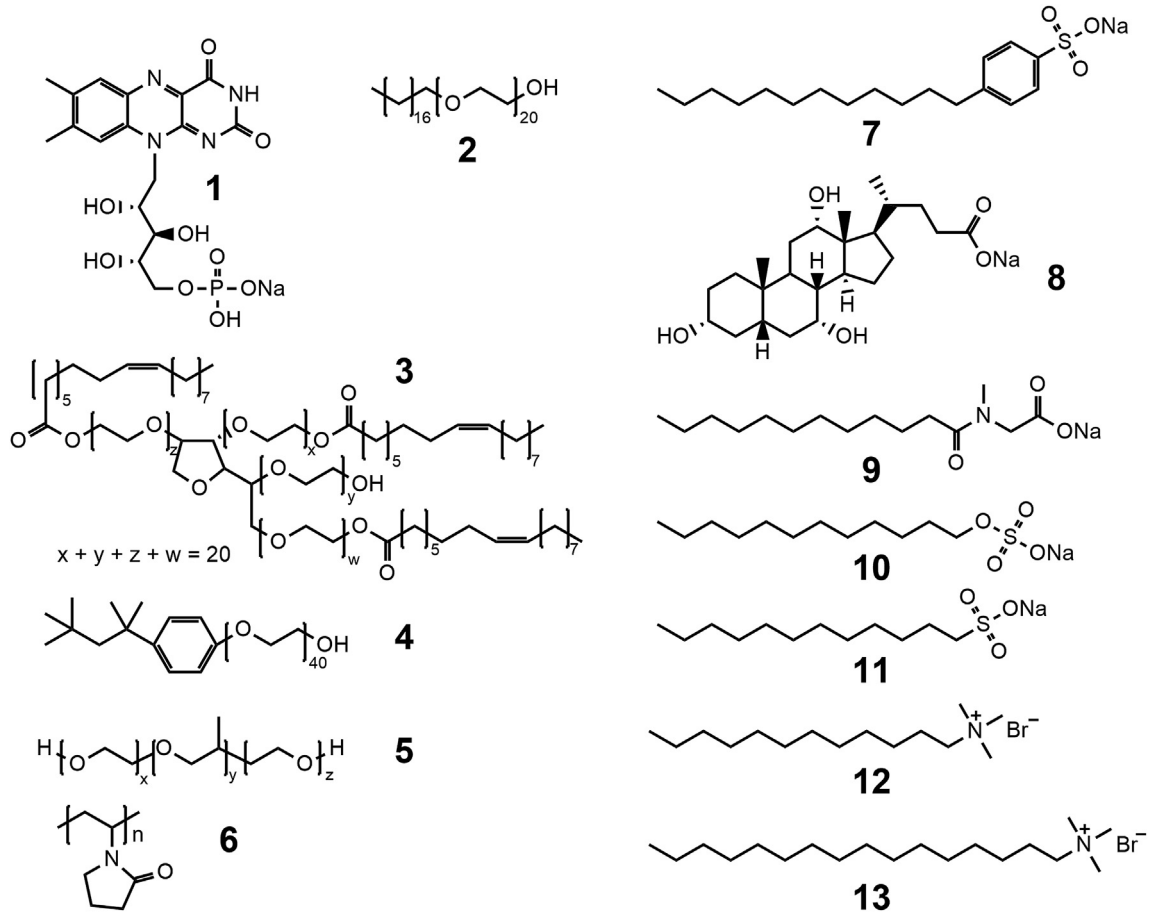

Fig. 1. Chemical structures of the main surfactants used in this study[†].

SWNTs is intrinsically related to K_d. Moreover, the micelle aggregation number (γ), which decides the size and shape of the micelle [28], is another important aspect in determining the surfactant organization and interaction with SWNTs. Among the various methods to probe the interaction among different surfactants [29–31], nuclear magnetic resonance (NMR) spectroscopy has been instrumental in shedding more light on the local structure and dynamics of the surfactant [30,31]. Therefore, detailed analysis of K_d and γ values of various surfactants will help in understanding the underlying SWNT sorting mechanism and enable to develop new method in a rational manner.

In this study, we quantitatively determined the K_d and γ of nine surfactants, including nonionic and anionic surfactants. Sensitive PL-based titrations using an FMN-SWNT dispersion against those surfactants allowed us to probe the surfactant assembly behavior near the SWNTs and to determine K_d and the related γ according to the SWNT chirality, handedness, and diameter (d_t). The origin of the K_d and γ of the SWNT was discussed by utilizing the hydrodynamic volume, γ, and hydrophobicity of the surfactant.

2. Experimental

2.1. Materials and instrumentation

Flavin mononucleotide (FMN, Lot #: 77623, purity: 73–79%), SDBS (technical grade), Pluronic F108, Triton X-405, and Brij 78 were purchased from Sigma-Aldrich. CTAB was purchased from Alfa Aesar. Other surfactants were purchased from TCI. SWNTs prepared by a high-pressure CO process (HiPco, raw grade, batch #: R1-831, with d_t distribution 1.00 ± 0.35 nm) were purchased from Nanointegris. UV–vis– near IR (NIR) absorption spectra were acquired on a JASCO 770 with a cuvette having a 10-mm beam path at 18 °C, unless otherwise noted. Tapping-mode atomic force microscope (AFM) measurements were conducted by using Nanowizard I (JPK Instruments) with an Al-coated Si cantilever with a resonance frequency of 361 kHz.

2.2. FMN-SWNT dispersion

A mixture of 20 mg (1.66 mmol in carbon atom equivalency) HiPco SWNT, 320 mg (0.7 mmol) FMN was added to 80 mL H_2O. The mixture was initially bath sonicated for 1 h and probe sonicated for 5 h at a 300-W intensity. The resulting solution was centrifuged at 80,000 g (gravitational acceleration force) for 2 h using a swing-bucket rotor (SW 41 Ti, Beckman Coulter), and the supernatant of the upper 80% was collected as a clear but dark solution. A total of 64 mL was prepared in this method. Prior to the optical measurements, the stock dispersion was prepared by seven-time dilution with DI water and contained *ca.* 1.2 mM FMN.

2.3. Cosurfactant-SWNT dispersions

SWNT dispersions using the surfactants displayed in Fig. 1 were prepared using the following method. A mixture of 1 mg (83 μmol in carbon atom equivalency) HiPco, 1 w/v% (10 mg) surfactant was added to 1 mL H_2O. The dispersion was initially mixed by vortexing,

bath sonicated for 5 min (Branson 1510, 70 W), and probe-sonicated for 1 h at a 300-W intensity to achieve thorough dispersion. The resulting solution was centrifuged at 122,000 g for 4 h using the aforementioned rotor and the 80% supernatant was collected to have a clear but dark solution. In the case of SDS, the pH of the dispersion was adjusted to 10. Each dispersion was subjected to UV-vis-NIR absorption and PL excitation (PLE) measurements.

2.4. PLE measurements and titration

Fluorescence spectroscopy measurements were conducted on a Spex Nanolog 3–211 spectrofluorometer equipped with a single-channel InGaAs detector and iHR320 spectrometer with 150 lines/mm grating. Cosurfactant titration against FMN-SWNT (3 mL) was conducted by increasing concentration in intervals as small as 1 nM (*i.e.*, PVP-1300) to 0.1 mM (*i.e.*, 4 μL, other surfactants) prior to measurement of the PLE map, according to the previous work [21]. All titration was conducted at 293 K, and both excitation and emission light intensities were corrected against instrumental variations using sensitivity correction factors. The ranges of excitation wavelength and emission wavelength were 550–800 nm in 5-nm steps and 903–1350 nm in 1-nm steps, respectively. After the titration, the dispersions exhibit near neutral pH at 7.7.

2.5. Relative K_d using the Hill equation

A PLE map array was imported to generate concentration-dependent traces of the PL intensity (I_{PL}) using the previously determined PL positions of SWNT (*n, m*) [21,32]. K_d and γ of cosurfactant were obtained using the Hill function implemented in Origin program.

3. Results and discussion

Fig. 1 displays the chemical structures of the main surfactants used in this study. These surfactants are classified as anionic, nonionic, and cationic (see Table S1 of the Supporting Information (SI) for the detailed properties of each surfactant). The majority of these surfactants are anionic surfactants (Figure nos. **1**, **7**–**11**), which have various functional tails comprising phosphate, carboxylate, sulfate, and sulfonate functionalities. The next most abundant surfactants are nonionic polymer with PEO repeat as the major hydrophilic part (nos. **2**–**5**), except the pyrrolidone moiety (no. **6**). The cationic surfactants were selected to have quaternary ammonium salt surfactants (nos. **12** and **13**). Generally, the hydrophobic parts of the dispersants consist of a long fatty chain ($n = 10$–18) with optional aromatic rings (nos. **4** and **7**), except in the case of Pluronic F108 (**5**) having polypropylene repeat.

† Anionic surfactants: **1**. FMN; **7**. sodium dodecylbenzene sulfonate (SDBS); **8**. SC; **9**. sodium dodecanoyl sarcosine (Sarkosyl); **10**. SDS; **11**. sodium dodecyl sulfonate (SDSA). Nonionic surfactants: **2**. Brij 78; **3**. Tween 85; **4**. Triton X-405, **5**. Pluronic F108, **6**. poly(vinyl pyrrolidone) (PVP-1300). Cationic surfactants: **12**. dodecyltrimethylammonium bromide (DTAB); **13**. cetyltrimethylammonium bromide (CTAB); The FMN-SWNT dispersion showed the most redshifted optical transitions among the SWNTs dispersed by the various surfactants listed in Fig. 1 and was utilized as a reference dispersion for the surfactant displacement. For this, the FMN-SWNT dispersion was prepared by using FMN and HiPco SWNTs (tube d_t range: 0.7–1.3 nm) [33] *via* the sonochemical method according to a previous report (see Section 2, Experimental for details) [32,34]. Using a similar sonochemical method, the remaining 12 surfactants, whose dispersion concentrations exceeded the critical micelle concentration (CMC) (see Table S1 for CMC values of each surfactant) [35–40], were prepared to disperse HiPco. The resulting FMN-HiPco dispersion exhibited high optical density and was diluted prior to measurement. Fig. 2A displays the UV-vis–NIR absorption spectra of the nanotube dispersed by 13 different surfactants normalized by the peak at *ca.* 1100 nm (see Fig. S1A to S1M in the SI for the absorption spectra without normalization). The FMN-HiPco dispersion (top spectrum) exhibit that the visible and NIR regions contain sharp absorption peaks that originate from the hydrogenic exciton peaks of the (*n*, *m*) SWNT chiralities [41] consisting of the first (e^S_{11}, 950–1350 nm) and second (e^S_{22}, 500–950 nm) excitonic transition regions of the FMN-wrapped SWNTs [21]. As mentioned, the excitonic peak of the SWNT displayed a blueshift upon dispersion with surfactants other than FMN because the ε_{eff} value was lowered by the hydrophobic alkyl chain as opposed to that of the fused aromatic ring structure of FMN [42]. As indicated by the dotted line, the excitonic peaks of the FMN-SWNT complex exhibit the most redshifted e^S_{11} peaks compared to those based on other surfactants. For example, the composite e^S_{11} peak at 1160 nm consisting of (9,4), (8,4), and (7,6) tubes displays a progressive 40-meV blueshift for the SDS (**10**)-SWNT dispersion, and the e^S_{22} peak near 730 nm shows a similar trend. In addition, judged by the absorbance, SDBS displays the densest SWNT dispersion, followed by SDS, FMN, SC, and cetyltrimethylammonium bromide (CTAB) in that order (see Fig. S1 for absorption without normalization).

The PL positions of (*n*, *m*) SWNT wrapped by various surfactants were determined by PLE maps because the respective I_{PL} during the titration of cosurfactants can be more easily determined than by the congested absorption spectra. Fig. S2 in the SI shows the PLE maps of HiPco dispersed by various surfactants, and these exhibit blueshifted e^S_{11} and e^S_{22} of SWNT compared to the FMN dispersion. The PL positions are listed in Table S2 in the SI. The determined PL positions of the (6,5) tubes shown in Fig. 2B displayed that while SDS suspended (6,5) tube displays the most blueshifted e^S_{11} and e^S_{22}, the FMN suspended (6,5) shows the most redshifted ones. The slight discrepancy between PL and absorption measurements (*e.g.*, SDS-HiPco displaying the second largest redshift) seems to originate from the presence of SWNT bundles [43,44]. A comparison of the PL positions from our experiments to those in the literature [34] (see Fig. S3 in the SI) reveals a similar optical transition trend, except for the cases of a slight mismatch for Tween 85 and Brij 78. The apparent redshift of the FMN-HiPco dispersion was advantageously utilized to detect the changes during titration.

Using the obtained PL positions of the SWNT, the chirality-specific I_{PL} were obtained for various surfactants to determine the relative K_d following a literature method (see Section 2, Experimental for the details) [21,32,45]. Initially, the time scale of surfactant replacement was probed whether any kinetics are involved in the replacement. For this, a series of PL emission spectra with 4 s intervals was acquired upon the addition of excess SDBS (*i.e.*, 1.7 mM) above CMC [39]. Fig. S4A in the SI illustrates PL emission spectra of (7,5) tube acquired after the addition. The corresponding I_{PL} trends of respective SDBS- and FMN-(7,5) tubes (Fig. S4B in the SI) exhibits saturation behavior after few tens of sec, and that of other chiralities such as (8,6) tube exhibiting the strongest binding with FMN [21] also does similar yet slightly delayed saturation behavior (Figs. S4C and D in the SI), suggesting kinetic replacement behavior according to SWNT chirality. Since the time scale of PLE maps are ~10 min which is much longer than that of replacement kinetics, we further collect PLE maps to obtain K_d according to titrant concentration. Typically, a titration of FMN-HiPco with a rough concentration interval of cosurfactant proceeded with initial 30 PLE map measurements and additional fine measurements in which the I_{PL} changed abruptly. The series of PLE maps with the determined PL positions enables the tracking of multiple SWNTs simultaneously according to the FMN- and titrant-based PL

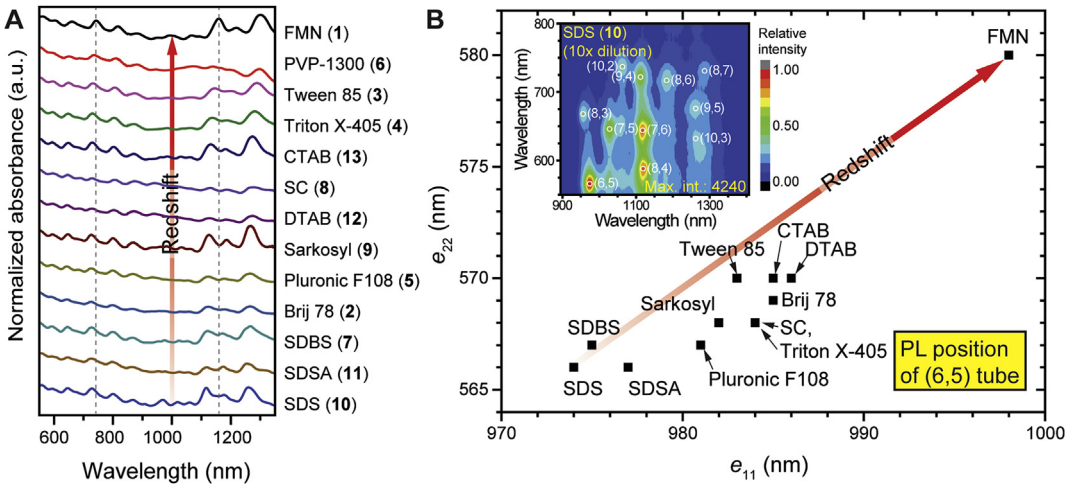

Fig. 2. (A) Normalized absorption spectra of the HiPco dispersion dispersed by various surfactants. (B) PL positions of a representative (6,5) tube were determined from PLE mapping (inset: SDS-HiPco dispersion) according to the dispersing surfactants. See Fig. S2 and Table S2 for the remaining PLE maps and the corresponding PL position for each surfactant, respectively. (A colour version of this figure can be viewed online.)

positions of the SWNTs. This process was repeated for the remaining 11 different surfactants. Fig. 3A displays a series of representative local PLE maps for the (7,5) tube upon the addition of Tween 85 aliquot. With increasing titrant concentration, as shown by the PLE maps (*i.e.*, 0.00, 0.09, and 0.18 mM from left to right), the I_{PL} of FMN-(7,5) progressively disappeared, whereas that of Tween 85-(7,5) rose in the blueshifted position, as indicated by the dotted line. Moreover, FMN-(7,5) positioned at 0.09 mM was also slightly blueshifted by a few nanometers in both e^S_{11} and e^S_{22} compared to the initial values.

The respective I_{PL} trajectories are displayed in Fig. 3B–J. Fig. 3B displays the I_{PL} trajectories of the (7,5) tube wrapped by FMN (black squares) and Pluronic F108 (red circles) during the replacement. The two I_{PL} drops, denoted regime I and II, were observed along the FMN-(7,5) trajectory, while that of Pluronic F108-(7,5) displays a small initial fluctuation and later a larger increase at those regimes. The initial I_{PL} drop has been discussed in a later section in detail. The latter accompanies the simultaneous increase in the I_{PL} of the Pluronic F108-SWNT, indicating the surfactant replacement. The commonly observed sigmoidal inflection of the respective I_{PL} values

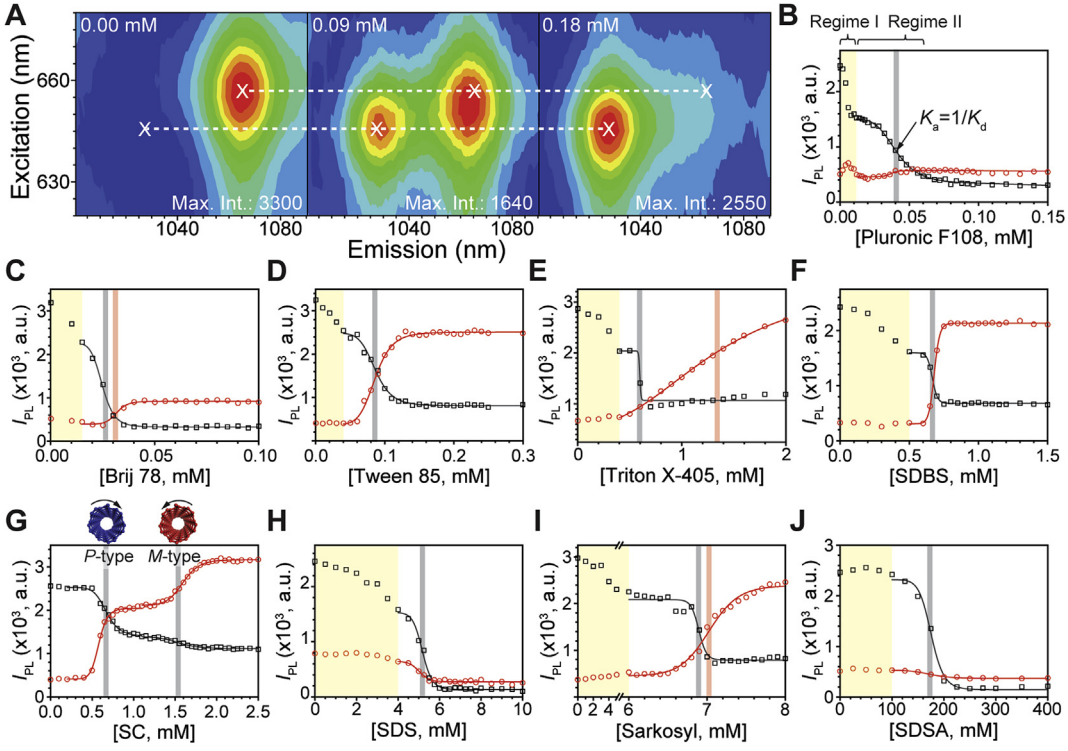

Fig. 3. I_{PL} trajectories of a representative (7,5) tube wrapped by FMN (black) replaced by various titrants (red). (A) A series of local PLE maps of (7,5) tubes upon the titration with Tween 85 (**3**). (B) I_{PL} trajectories of (7,5) tubes measured at the respective surfactant positions for Pluronic F108 (**5**) and similar trajectories for (C) Brij 78 (**2**), (D) Tween 85 (**3**), (E) Triton X-405 (**4**), (F) SDBS (**7**), (G) SC (**8**), (H) SDS (**10**), (I) Sarkosyl (**9**), and (J) SDSA (**11**). (A colour version of this figure can be viewed online.)

can be quantified by Hill analysis [21,46]. The Hill equation is expressed as

$$\theta = \left[\left(\frac{K_a}{[titrant]}\right)^{\gamma} + 1\right]^{-1}, \quad (1)$$

where K_a is the middle point of the sigmoidal transition, θ is fraction based on the I_{PL} of FMN- and titrant-SWNTs, and γ is a Hill coefficient representing surfactant cooperativity. Since K_a denotes the affinity of FMN with SWNT, the reciprocal K_a (or K_d) results in the relative binding affinity of various surfactants. The determined K_a and γ values for various surfactants are listed in Table S3 in the SI. Fig. 3C through J display the similar I_{PL} trajectories of the other eight titrants. The reason for being slightly different I_{PL} of FMN-derived (7,5) tube after the titration stems from (*i*) the contribution of I_{PL} and peak width of cosurfactant-SWNT after titration, and (*ii*) different degree of overlapping of (7,5) tube with (10,2) tubes (see Fig. 3A for Pluronic F108 and Fig. S5 for the other surfactants in the SI). During the titration of various titrants, although the anionic and nonionic surfactants allowed the observation of the PL position changes of SWNTs without apparent precipitation, the cationic surfactants (*e.g.*, DTAB (**12**) and CTAB (**13**)) display SWNT precipitation at *ca.* one-tenth (0.1–0.2 mM) the molar concentration of FMN in the dispersion. This result occurs because of a salt-forming reaction between the anionic and cationic surfactants [32,47]. Therefore, these cationic surfactants are not discussed further.

The simultaneous I_{PL} changes in regime II were first probed. Upon titration, the I_{PL} of the (7,5) tube wrapped by FMN and subsequently replaced by the titrants displayed the following three behaviors: (*i*) FMN is complementarily displaced by the titrant and immediately forms a stable dispersion (*i.e.*, in the cases of titration with Pluronic F108 (**5**), Tween 85 (**3**), SDBS (**7**), and SC (**8**)). (*ii*) Displacement induces small SWNT bundling, as determined from the simultaneous PL decrease without noticeable precipitation observable to the naked eyes (*i.e.*, SDS (**10**) and sodium dodecyl sulfonate (SDSA) (**11**)) [21]. (*iii*) Displacement occurs immediately, and a subsequent, slow I_{PL} increase in the PL position of the titrant-SWNT occurs, as shown by the difference in the gray and red regions (*i.e.*, Brij 78 (**2**), Triton X-405 (**4**), and Sarkosyl (**9**)). The behavior of surfactant replacement has a close relationship with micelle relaxation time ($\tau_{micelle}$), which is defined as the time for micelle to be relaxed after the addition of the surfactant monomer [48–50]. Generally, $\tau_{micelle}$ of an anionic surfactant is in the range of seconds to microseconds, whereas those of nonionic surfactants are much longer (a few tens of seconds) because of the presence of the polar head group, which directs organization. Immediate surfactant exchange based on the simultaneous I_{PL} changes are observed for cases (*i*) and (*ii*), which has been observed for SDBS, SC, and SDS already, in good agreement with the short $\tau_{micelle}$ [21]. At this time, case (*iii*), mainly from nonionic surfactants, has been observed for the first time. Case (*iii*) suggests that the replaced surfactant requires surfactant rearrangement on the SWNT to obtain a well-ordered surfactant structure based on the slow PL recovery. In the case of Triton X-405, the time for $\tau_{micelle}$ to reach the PL plateau was about 50 min, which is far greater than that of (*i.e.*, a few tens of seconds) the typical nonionic surfactants [49], inferring the importance of kinetic aspects of nonionic surfactant rearrangement. This also suggests that the hydrophobicity of the SWNT sidewall prevents the self-organization of several nonionic surfactants. In addition, it is noteworthy that several surfactants such as SDBS and SC exhibits two sigmoidals, which originate from different interactions of FMN with minus (*M*) and plus (*P*)-helices of the SWNT isomers (see Fig. 3G and Figs. S6E and F for their K_d) [26,51].

In regime I, moreover, the I_{PL} trajectories from FMN-SWNT exhibit an initial PL decrease (yellow shaded region) although the I_{PL} of the counterpart shows silent responses, except for the SC case, and is devoid of regime I behavior. Because the replacement occurs based on the difference in K_d, this result indicates that two different surfactant organizations, namely defective *vs.* defect-free, exist as shown in the schematic in Fig. 4A [21,52]. Defective assembly is the imperfect organization of the FMN assembly on the SWNT sidewalls. In regime I, the titrant surfactants are attached at defect assembly on SWNT, and the I_{PL} originating from partial FMN wrapping continuously decreases, although the I_{PL} of the titrant-SWNT does not increase. The local adsorption of the titrant affects the FMN-SWNT PL position, as evident by the initial slight blueshift in the PLE map shown in Fig. 3A. In regime II, the titrant completely replaces the FMN wrapping in both defect-free and defective assemblies.

In order to obtain insight, the absorption-based titration of SDBS against FMN-HiPco (Fig. 4B) was conducted. It revealed that, in regime I, the absorbance of (7,5) tubes increases along with peak broadening without changing peak maximum. The fact that peak broadening at same wavelength indicates the increase of heterogeneous environment around SWNT such as inclusion of SDBS. Moreover, since exciton diffusion length is typically 90 nm for SWNT with 1-nm d_t [53], if SDBS makes larger micellar domain than exciton diffusion length on SWNT, exciton would dissociate with lower e^S_{11} owing to SDBS environment. However, in regime I, we did not observe new absorption appearance at SDBS-(7,5) position, inferring the absence of larger SDBS domain. In regime II, the (7,5) peak was blueshifted to 1028 nm with additional 1061-nm peak which originates from SDBS-replaced (10,2) peak. This result infers that in regime II SDBS makes larger micellar domain exceeding the exciton diffusion length. Those trends also were observed other chiralities as well (see Fig. S7 for whole absorption spectra). In fact, the AFM image of FMN-HiPco on mica in Fig. 4C shows that the helical FMN wrapping on SWNT [32] is not entirely uniform along the sidewalls of SWNT. The height of FMN-HiPco is *ca.* 2.2 nm. AFM image of the sample from regime I which was prepared by careful few washings with DI water (Fig. 4D) displays that large SDBS aggregates with 10–20 nm height on top of *ca.* 3.8 nm tall FMN-HiPco were decorated preferentially at the ends along with the middle part. It is noteworthy that careful washing is necessary to obtain preserved surfactant morphology. This result clearly indicates that FMN on SWNT at regime I is partially replaced by SDBS, presumably owing to weak binding affinity with the existing surfactant. AFM image from the sample after regime II (Fig. 4E) displays 8.4-nm tall, non-periodic bumpy morphologies which exhibit distinct departure from the initial periodic helical FMN wrapping and suggest hemimicelle of SDBS. AFM imaging along with absorption measurement provide ample evidences for the defective and defect-free arrangement of the surfactant. If the aforementioned defective and defect-free structures exist, prolonged incubation produces more stable structure owing to dynamic equilibrium of surfactant and subsequent healing. To confirm this point, the FMN-HiPco sample was aged for 30 days (denoted “aged sample”) to induce the healing of the surfactant organization and then compared to the initial values. Fig. 4F shows the I_{PL} traces of SDBS titration using the initial (black) and the aged (red) samples. Clearly, the K_a of the aged sample increases by 0.05 mM, indicating a tighter interaction between FMN and SWNT with aging. Moreover, the middle point in regime I also increases as well, suggesting the rearrangement of the defective molecule over time. Along the AFM measurements, this result strongly supports the existence of defective and defect-free region on the SWNTs.

The K_d of various surfactants could be quantitatively compared because the same FMN-HiPco dispersion was utilized. Fig. 5A and B

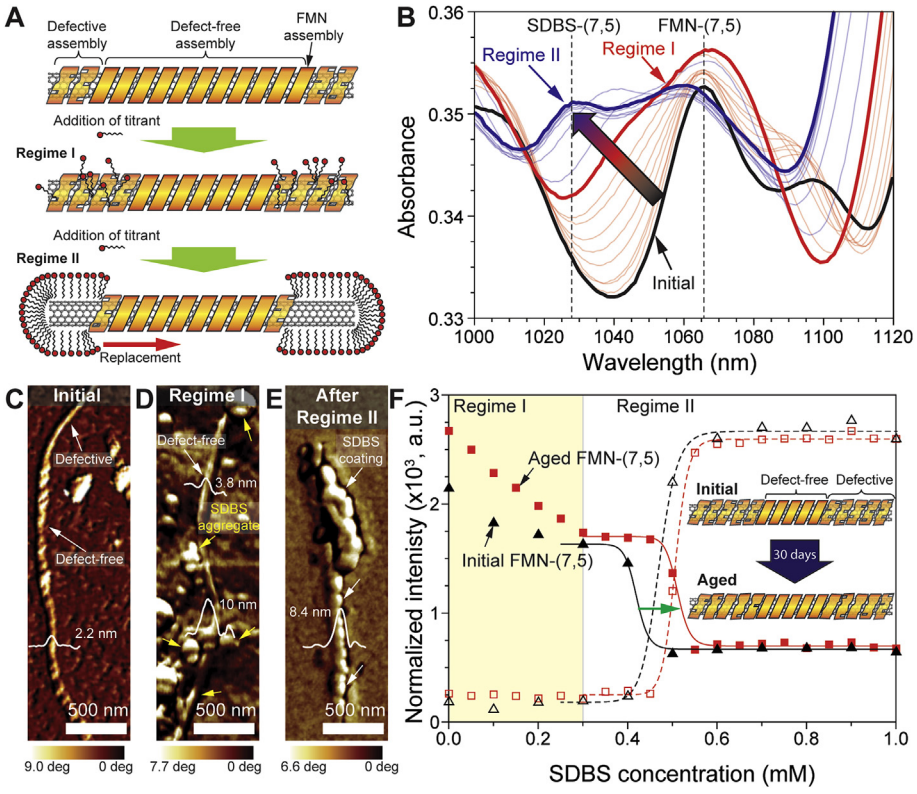

Fig. 4. (A) Schematics of defective and defect-free FMN organizations on SWNT and subsequent replacement with titrant. (B) Absorption change of FMN-(7,5) tube upon the titration of SDBS indicated by arrow. AFM phase images of the samples obtained at (C) the initial, (D) the regime I, and (E) after the regime II stages. (F) Binding affinity difference of FMN-HiPco for the initial and aged samples against SDBS titration. Solid triangle and square symbols denote I_{PL} of the initial and aged FMN-(7,5) tubes, and corresponding empty symbols indicate the respective I_{PL} of SDBS-replaced (7,5) tubes. (A colour version of this figure can be viewed online.)

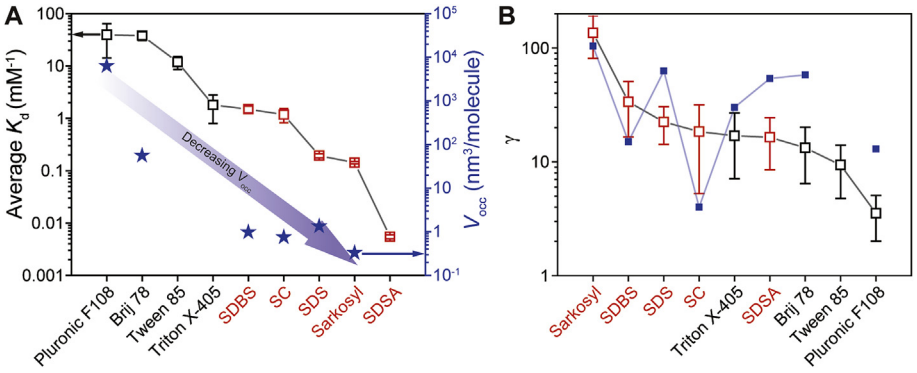

Fig. 5. Comparison of K_d and γ of various surfactants with SWNT. (A) The average K_d (left axis) and V_{occ} (star symbol, right axis) according to surfactants. (B) γ of the various nonionic (black) and anionic (red) surfactants in the presence (empty square) or absence (solid square) of SWNTs. Bar indicates the standard deviation arising from SWNT chiralities. (A colour version of this figure can be viewed online.)

illustrate the average K_d (the left *y*-axis), the calculated occupied volume per surfactant molecule (V_{occ}, the right *y*-axis), and γ of various surfactants determined for various SWNT chiralities (see Tables S4 and S3 in the SI for K_d and γ, respectively, from each surfactant). The order of average K_d is Pluronic F108 (**5**) > Brij 78 (**2**) > Tween 85 (**3**) > Triton X-405 (**4**) > SDBS (**7**) > SC (**8**) > SDS (**10**) > Sarkosyl (**9**) > SDSA (**11**). Overall, the nonionic surfactants (black) with a polymeric PEO repeat have higher K_d than anionic surfactants (red). Remarkably, the average K_d (*i.e.*, *ca.* 39 mM^{-1}) of Pluronic F108 is nearly four orders of magnitude higher than that (*i.e.*, *ca.* 0.005 mM^{-1}) of SDSA. In addition, γ which defines the number of molecules in a micelle [54] was simultaneously obtained. Fig. 5B illustrate γ trend in the presence (empty) and absence (solid) of SWNT. There is a weak correlation between two γ values, suggesting that micellar structure in the presence of SWNT undergoes large deviation as compared to the bare micellar structure. The value of γ decreases in the following order: Sarkosyl (**9**), SDBS (**7**), SDS (**10**), SC (**8**), Triton X-405 (**4**), SDSA (**11**), Brij 78 (**2**), Tween 85 (**3**), and Pluronic F108 (**5**). The general trend is that small and molecular anionic surfactant (red) with normal aliphatic chain have a larger γ (from 16 to 135) than those (from 3 to 16) of nonionic polymeric surfactants (black) with PEO units. Moreover, the surfactants on SWNT exhibit lower γ values than the bare micelles, except for SC and SDBS [55–62]. Those surfactants having

higher γ value than those in bare micelle state (*i.e.*, SC and SDBS) often have strong hydrophobic interactions caused by aromatic or steroidal structures. The deviation seems to originate from the drastic increase in surfactant cooperativity or aggregation number (*i.e.*, micelle to tubular structure) owing to the strong hydrophobic interactions with the underlying graphene sidewalls [23,63]. We also extracted the K_d patterns of various surfactants according to d_t, as shown in Figs. S6A–I. The linear regression of the chirality-dependent K_d values according to d_t revealed the rough larger d_t preference of Pluronic F108, along with similar trend for Brij 78, Sarkosyl, and SDSA (corresponding to Figs. S6A, B, H, and I, respectively). The other surfactants such as SDBS and SC (Figs. S6E and F) exhibit preferences for the smaller-d_t SWNT. The remaining surfactants including Tween 85, Triton X-405, and SDS (Figs. S6C, D, and G, respectively) display similar affinities for all SWNT chiralities.

We found that SWNT wrapped by nonionic surfactants exhibits lowered PL (*i.e.*, Pluronic F108 and Brij 78) after titration compared to that wrapped by FMN, except for the case of SWNT bundling (*i.e.*, SDS and SDSA). A possible reason for these PL results might be the change in (*i*) the chirality abundance of SWNT during surfactant exchange or (*ii*) the ε_{eff} or local pH of the immediate environment [25,64]. There is little difference in the chirality abundance from surfactant to surfactant after titration, as shown in the PLE maps in Figs. S5A–J in the SI. The corresponding histograms of SWNT chiralities (Figs. S8A–I in the SI) show a similar trend, showing (8,4) and (7,6) as the major species. Therefore, the possibility of SWNT abundance changes was excluded. Next, we probed the effect of local pH changes of the SWNTs. For this, the titrated sample having neutral pH at 7.7 was further basified to pH 10 to see the optical changes. Fig. S9B in the SI shows the absorption spectra of an FMN-HiPco dispersion (black) titrated with 0.2 mM Pluronic F108 before (red) and after (blue) the addition of a NaOH solution. It is well known that increasing the pH reduces the peroxide concentration as a result of the reactions of protons with oxygen in the presence of electrons and creates reversible endoperoxide defects on SWNT [64,65]; therefore, increasing the pH results in an increase in the PL of the SWNT. However, our experimental results show a slight increase in PL for SDS-HiPco (Fig. S9E) but slightly lowered PLs for the other surfactants (*i.e.*, Brij 78 and SC in Figs. S9D and F, respectively) or drastically decreased PL (Pluronic F108 in Fig. S9C). This result indicates that, unlike the previous report [64], the change in I_{PL} upon pH change is dependent on a possible change in the surfactant organization on the SWNT sidewalls owing to anionic repulsion [66]. For instance, it was reported that the periodic spacing of SDS hemi-micelle on highly oriented pyrolytic graphite surface shrinks with higher ionic strength owing to increased ε_{eff} and subsequent reduction in Coulombic interaction [67]. The reduced spacing also leads to tight surfactant wrapping, leading to undoped SWNT which is more inert to environment. In this regard, as evident by FMN to SC replacement, and subsequent pH change does not change I_{PL} much. This seems to originate from tight wrapping structure provided by both FMN and SC [45,68]. This experiment supports that the different I_{PL}s after the titrations seem to relate to the different response on the surfactant tightness.

In order to understand the role of SWNTs associated with surfactant, K_a values of the titrants were compared to the reported CMC values of bare surfactants [35–40]. Fig. 6 displays the plot of K_a and CMC. Overall, K_a exhibits similar or slightly lower than CMC except the cases of Tween 85 and SDSA. The result indicates that K_a is considered as CMC in the presence of SWNT. The fact that overall K_a has slightly lower than CMC without SWNT infers that SWNT facilitates the assemblage of surfactants at lower concentration owing to the hydrophobic interaction between its sidewalls and hydrophobic tails. Especially, K_a of Pluronic F108 and SC cases are

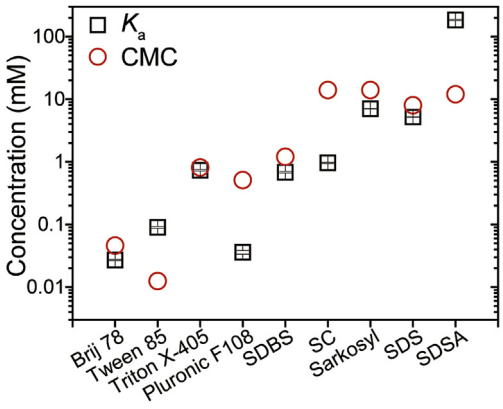

Fig. 6. Comparison of the determined K_a of various surfactants in presence of SWNT and the reported CMC values without SWNT. Standard deviations are denoted as bar. (A colour version of this figure can be viewed online.)

nearly ten fold smaller as compared to their bare states. It was documented that SDBS and SDS in the presence of SWNT display lower CMC than their bare states do [69], supporting the promoted micellization by SWNT. It is noteworthy how the chemical nature of surfactant affects K_a. With a same end group (*i.e.*, sulfonate), SDBS which has additional benzene ring as compared to SDSA increased K_a over three orders of magnitude higher [56]. With same chain length, different head groups (*i.e.*, sulfate and sulfonate of SDS and SDSA, respectively) also give 36 times difference in K_a. Moreover, since K_a is equal to [FMN]/K where K is equilibrium constant [21,22], Gibbs energy changes (ΔG) has been obtained. Using the equation $\Delta G = -RT \ln K$ where R and T are a gas constant (8.314 J/mol•K) and temperature in Kelvin, we plotted K *vs* ΔG as shown in Fig. S10 in the SI. The most negative ΔG from FMN to cosurfactant replacement was obtained from Pluronic F108, showing the average ΔG −9.4 kJ/mol, and are in the order of Brij 78, Tween 85, Triton X-405, SDBS, and SC. Positive ΔG were obtained from SDS, Sarkosyl, and SDSA whose ΔG values are in accordance with the previous report [21].

Overall, on top of the chemical nature of surfactant, the molar K_d of the surfactants with SWNT seems to be dependent on the nature of the surfactant assembly, that is, the hydrodynamic volume, aggregation number, and hydrophobic/philic parts. Generally, anionic surfactants exhibit smaller K_d values compared to nonionic ones. Similarly, anionic surfactants exhibit large γ, in which anionic surfactants typically forms spherical micelles or similar structures (*i.e.*, elongated prolated micelle) [10,48,70,71]. For example, based on the reported hydrodynamic volume of SDS (*i.e.*, 1.9 nm in diameter) [72] and the determined γ (*ca.* 22, see Table S3), the calculated V_{occ} is about 1.37 nm^3/molecule. This value is about three orders of magnitude smaller than that (*i.e.*, 6360 nm^3/molecule) of Pluronic F108, mainly owing to the relatively smaller V_{occ} and larger γ. Thus, we plotted V_{occ} with K_d simultaneously, as shown in Fig. 5A, in which several V_{occ} values were omitted owing to limited availability of hydrodynamic volumes for several surfactants (see Table 1) [55,56,72–74]. The V_{occ} trend is in accordance with the observed K_d trend, indicating that the molar hydrodynamic volume is key to the molar K_d.

Fig. 7 illustrates the representative cartoons for anionic and nonionic surfactant arrangements in the absence and presence of SWNTs. Anionic surfactants with long *n*-alkyl chains are prone to form a more closely packed structure owing to van der Waals interactions, as shown in Fig. 7A. In contrast, nonionic surfactants with a PEO repeat (Fig. 7B) possess loose hydrated structures because of their polymeric nature [75]. Therefore, the closely-

Table 1
Calculated V_{occ} based on hydrodynamic volume and γ using the reported micelle radius [55,56,72–74].

Surfactant type	Surfactant	Micelle radius (nm)	Average γ	Calculated V_{occ} (nm^3/molecule)[a]
Nonionic	Pluronic F108 (**5**)	17.5	3.5	6360
	Brij 78 (**2**)	5.7	13	57
Anionic	SDBS (**7**)	2.0	34	1.0
	SC (**8**)	1.5	18	0.8
	SDS (**10**)	1.9	22	1.3
	Sarkosyl (**9**)	2.2	136	0.3

[a] V_{occ} was calculated by the following equation: $[(4/3) \times \pi \times (\text{micelle radius})^3]/\gamma$.

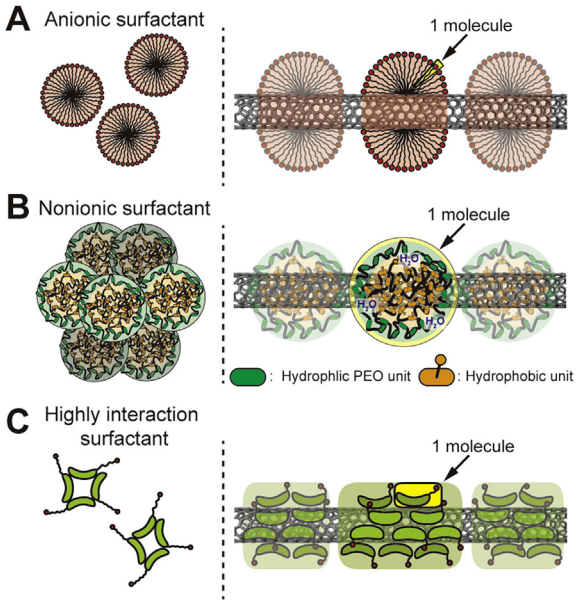

Fig. 7. Illustrations of the proposed model to understand the difference in relative K_d. Morphologies of (A) micellar anionic surfactants, (B) nonionic surfactants with PEO repeat units, and (C) highly interacting surfactants with SWNT in the absence (left) and presence of SWNTs, respectively. Yellow shading denotes the V_{occ}. (A colour version of this figure can be viewed online.)

packed aggregates of anionic surfactant have a lower local ε_{eff} near the SWNT compared to that of the hydrated, loosely-organized nonionic surfactants. Surfactants that interact strongly with SWNT change their structure in the presence of SWNTs. The organized structure changes from micellar to tubular in the absence and presence of SWNTs, as evident by the change in γ in Fig. 5B. These variations in surfactant structure seem to correlate with the different I_{PL} values upon surfactant exchange. The determination of the hydrodynamic volume of surfactant micelles on SWNTs would be highly desirable to obtain accurate γ values for the SWNT.

The determination of the relative K_d and the behavior on the nanotube surface according to their ionic properties of various surfactant provide an insight into the underlying mechanism of SWNT sorting. First, Arnold et al. [1] reported that SWNT separation by DGU method is enhanced by the use of a 1:4 mixed SDS/SC system rather than SC alone and showed that the larger d_t SWNTs move to a high-density area. Based on the higher K_d of SC with the SWNT than SDS (1.2 and 0.2 mM^{-1}) and the tubes with smaller d_t (shown in Fig. S6F in the SI) in our experiment, the larger d_t tube will experience partial surfactant replacement, which is in accordance with NMR experiments [31]. These results provide the reason that the (6,5) tube maintains a similar density, whereas a larger d_t SWNT moves to a higher density region [1] because of the partial surfactant replacement and subsequent density changes in the mixed surfactant-SWNT construct. In addition, Wang et al. [27] reported SWNT separation using a Triton X-405/SDBS system in which Triton X-405 was used as dispersant and SDBS was used to elute metallic SWNTs. The reason for such sorting originates from the similar K_d values (*i.e.*, Triton X-405: 1.8 mM^{-1}, SDBS: 1.5 mM^{-1}). The determined K_d values of various surfactants in our study opens up the possibility to explore various combinations of surfactants to develop a novel sorting scheme.

4. Conclusions

We determined the relative binding affinities and aggregation number of nine surfactants using the optical titration method using FMN-SWNT as a starting dispersant, which provided a quantitative comparison of surfactant exchange. The strong redshift induced by FMN allowed us to probe the local environment of the SWNT during the seamless surfactant exchange without bundling or precipitation. The exchange reaction monitored by the optical titration method using I_{PL} of SWNT proceeded with two regimes in which the first and second exchanges exhibit partial and full replacements of the existing surfactant, supported by absorption, PL, and AFM measurements. The second transitions allowed the measurement of the relative K_d (*i.e.*, Pluronic F108 > Brij 78 > Tween 85 > Triton X-405 > SDBS > SC > SDS > Sarkosyl > SDSA) and γ of various surfactants according to nanotube chiralities, and K_d of SWNT handedness in some cases. Nonionic surfactants display larger K_d and lower γ than those of anionic surfactants. This trend can be mainly explained by the occupied volume on the SWNTs, surfactant organization structure, and specificity of the hydrophobic part. The presence of SWNT promotes micellization for the most of surfactants, evident by similar or slightly lower K_a values than CMC of bare surfactants, and there are slight deviations depending on the structural characteristics of surfactants such as aromatics, and nature of head groups. This study provides the detailed concentration-dependent replacement behavior of two surfactants and an estimation of K_d of various surfactants along with fine tuning of surfactant organization, which is useful for designing a novel sorting scheme for SWNT.

Acknowledgments

This research was supported by the Basic Science Research Program through the gs1:National Research Foundation of Korea funded by the gs2:Ministry of Education, Science and Technology (NRF-2017R1D1A1A09000589).

Appendix A. Supplementary data

Supplementary data related to this article can be found at https://doi.org/10.1016/j.carbon.2018.07.003.

References

[1] M.S. Arnold, A.A. Green, J.F. Hulvat, S.I. Stupp, M.C. Hersam, Sorting carbon nanotubes by electronic structure using density differentiation, Nat.

Nanotechnol. 1 (1) (2006) 60–65.
[2] K. Yanagi, T. Iitsuka, S. Fujii, H. Kataura, Separations of metallic and semiconducting carbon nanotubes by using sucrose as a gradient medium, J. Phys. Chem. C 112 (48) (2008) 18889–18894.
[3] A.L. Antaris, J.-W.T. Seo, A.A. Green, M.C. Hersam, Sorting single-walled carbon nanotubes by electronic type using nonionic, biocompatible block copolymers, ACS Nano 4 (8) (2010) 4725–4732.
[4] S. Ghosh, S.M. Bachilo, R.B. Weisman, Advanced sorting of single-walled carbon nanotubes by nonlinear density-gradient ultracentrifugation, Nat. Nanotechnol. 5 (6) (2010) 443–450.
[5] M. Zheng, A. Jagota, E.D. Semke, B.A. Diner, R.S. McLean, S.R. Lustig, et al., DNA-assisted dispersion and separation of carbon nanotubes, Nat. Mater. 2 (5) (2003) 338–342.
[6] T. Tanaka, H. Jin, Y. Miyata, S. Fujii, H. Suga, Y. Naitoh, et al., Simple and scalable gel-based separation of metallic and semiconducting carbon nanotubes, Nano Lett. 9 (4) (2009) 1497–1500.
[7] H. Liu, D. Nishide, T. Tanaka, H. Kataura, Large-scale single-chirality separation of single-wall carbon nanotubes by simple gel chromatography, Nat. Commun. 2 (2011) 309.
[8] C.Y. Khripin, J.A. Fagan, M. Zheng, Spontaneous partition of carbon nanotubes in polymer-modified aqueous phases, J. Am. Chem. Soc. 135 (18) (2013) 6822–6825.
[9] J.A. Fagan, E.H. Hároz, R. Ihly, H. Gui, J.L. Blackburn, J.R. Simpson, et al., Isolation of >1 nm diameter single-wall carbon nanotube species using aqueous two-phase extraction, ACS Nano 9 (5) (2015) 5377–5390.
[10] M.J. O'Connell, S.M. Bachilo, C.B. Huffman, V.C. Moore, M.S. Strano, E.H. Haroz, et al., Band gap fluorescence from individual single-walled carbon nanotubes, Science 297 (5581) (2002) 593–596.
[11] C. Backes, S. Bosch, U. Mundloch, F. Hauke, A. Hirsch, Density gradient ultracentrifugation on carbon nanotubes according to structural integrity as a foundation for an absolute purity evaluation, ChemPhysChem 12 (14) (2011) 2576–2580.
[12] A.V. Naumov, S. Ghosh, D.A. Tsyboulski, S.M. Bachilo, R.B. Weisman, Analyzing absorption backgrounds in single-walled carbon nanotube spectra, ACS Nano 5 (3) (2011) 1639–1648.
[13] M.E. Itkis, D.E. Perea, S. Niyogi, S.M. Rickard, M.A. Hamon, H. Hu, et al., Purity evaluation of as-prepared single-walled carbon nanotube soot by use of solution-phase near-IR spectroscopy, Nano Lett. 3 (3) (2003) 309–314.
[14] Y. Liu, W. Lai, T. Yu, Y. Kang, Z. Ge, Interactions of carbon nanotubes with the nitromethane-water mixture governing selective adsorption of energetic molecules from aqueous solution, Phys. Chem. Chem. Phys. 17 (10) (2015) 6995–7001.
[15] S. Conti, M. Cecchini, Accurate and efficient calculation of the desorption energy of small molecules from graphene, J. Phys. Chem. C 119 (4) (2015) 1867–1879.
[16] Y. Wang, Theoretical evidence for the stronger ability of thymine to disperse SWCNT than cytosine and adenine: self-stacking of DNA bases vs their cross-stacking with SWCNT, J. Phys. Chem. C 112 (37) (2008) 14297–14305.
[17] S.M. Tomásio, T.R. Walsh, Modeling the binding affinity of peptides for graphitic surfaces. Influences of aromatic content and interfacial shape, J. Phys. Chem. C 113 (20) (2009) 8778–8785.
[18] G. Zuo, X. Zhou, Q. Huang, H. Fang, R. Zhou, Adsorption of villin headpiece onto graphene, carbon nanotube, and C60: effect of contacting surface curvatures on binding affinity, J. Phys. Chem. C 115 (47) (2011) 23323–23328.
[19] L.K. Boateng, J. Heo, J.R.V. Flora, Y.-G. Park, Y. Yoon, Molecular level simulation of the adsorption of bisphenol A and 17α-ethinyl estradiol onto carbon nanomaterials, Separ. Purif. Technol. 116 (2013) 471–478.
[20] J. Zhang, M.P. Landry, P.W. Barone, J.-H. Kim, S. Lin, Z.W. Ulissi, et al., Molecular recognition using corona phase complexes made of synthetic polymers adsorbed on carbon nanotubes, Nat. Nanotechnol. 8 (2013) 959.
[21] H. Oh, J. Sim, S.-Y. Ju, Binding affinities and thermodynamics of noncovalent functionalization of carbon nanotubes with surfactants, Langmuir 29 (35) (2013) 11154–11162.
[22] Y. Kato, A. Inoue, Y. Niidome, N. Nakashima, Thermodynamics on soluble carbon nanotubes: how do DNA molecules replace surfactants on carbon nanotubes? Sci. Rep. 2 (733) (2012) 1–7.
[23] F.F. Bergler, S. Stahl, A. Goy, F. Schöppler, T. Hertel, Substrate-mediated cooperative adsorption of sodium cholate on (6,5) single-wall carbon nanotubes, Langmuir 32 (37) (2016) 9598–9603.
[24] A. de Juan, A. Lopez-Moreno, J. Calbo, E. Orti, E.M. Perez, Determination of association constants towards carbon nanotubes, Chem. Sci. 6 (12) (2015) 7008–7014.
[25] J.H. Choi, M.S. Strano, Solvatochromism in single-walled carbon nanotubes, Appl. Phys. Lett. 90 (22) (2007) 223114.
[26] J. Sim, S. Kim, M. Jang, M. Park, H. Oh, S.-Y. Ju, Determination of the absolute enantiomeric excess of the carbon nanotube ensemble by symmetry breaking using the optical titration method, Langmuir 33 (41) (2017) 11000–11009.
[27] J. Wang, T.D. Nguyen, Q. Cao, Y. Wang, M.Y.C. Tan, M.B. Chan-Park, Selective surface charge sign reversal on metallic carbon nanotubes for facile ultrahigh purity nanotube sorting, ACS Nano 10 (3) (2016) 3222–3232.
[28] R.G. Alargova, I.I. Kochijashky, M.L. Sierra, R. Zana, Micelle aggregation numbers of surfactants in aqueous Solutions: a comparison between the results from steady-state and time-resolved fluorescence quenching, Langmuir 14 (19) (1998) 5412–5418.
[29] M.S. Arnold, J. Suntivich, S.I. Stupp, M.C. Hersam, Hydrodynamic characterization of surfactant encapsulated carbon nanotubes using an analytical ultracentrifuge, ACS Nano 2 (11) (2008) 2291–2300.
[30] S.-Y. Ju, M. Utz, F. Papadimitrakopoulos, Enrichment mechanism of semiconducting single-walled carbon nanotubes by surfactant amines, J. Am. Chem. Soc. 131 (19) (2009) 6775–6784.
[31] T.A. Shastry, A.J. Morris-Cohen, E.A. Weiss, M.C. Hersam, Probing carbon nanotube–surfactant interactions with two-dimensional DOSY NMR, J. Am. Chem. Soc. 135 (18) (2013) 6750–6753.
[32] S.-Y. Ju, J. Doll, I. Sharma, F. Papadimitrakopoulos, Selection of carbon nanotubes with specific chiralities using helical assemblies of flavin mononucleotide, Nat. Nanotechnol. 3 (6) (2008) 356–362.
[33] P. Nikolaev, M.J. Bronikowski, R.K. Bradley, F. Rohmund, D.T. Colbert, K.A. Smith, et al., Gas-phase catalytic growth of single-walled carbon nanotubes from carbon monoxide, Chem. Phys. Lett. 313 (1–2) (1999) 91–97.
[34] V.C. Moore, M.S. Strano, E.H. Haroz, R.H. Hauge, R.E. Smalley, J. Schmidt, et al., Individually suspended single-walled carbon nanotubes in various surfactants, Nano Lett. 3 (10) (2003) 1379–1382.
[35] C. Klammt, D. Schwarz, K. Fendler, W. Haase, V. Dötsch, F. Bernhard, Evaluation of detergents for the soluble expression of α-helical and β-barrel-type integral membrane proteins by a preparative scale individual cell-free expression system, FEBS J. 272 (23) (2005) 6024–6038.
[36] L.S.C. Wan, P.F.S. Lee, CMC of polysorbates, J. Pharmacol. Sci. 63 (1) (1974) 136–137.
[37] T. Tanaka, Y. Urabe, D. Nishide, H. Kataura, Discovery of surfactants for metal/semiconductor separation of single-wall carbon nanotubes via high-throughput screening, J. Am. Chem. Soc. 133 (44) (2011) 17610–17613.
[38] J.R. Lopes, W. Loh, Investigation of self-assembly and micelle polarity for a wide range of ethylene Oxide–Propylene Oxide–Ethylene oxide block copolymers in water, Langmuir 14 (4) (1998) 750–756.
[39] Y. Shi, H.Q. Luo, N.B. Li, Determination of the critical premicelle concentration, first critical micelle concentration and second critical micelle concentration of surfactants by resonance Rayleigh scattering method without any probe, Spectrochim. Acta 78 (5) (2011) 1403–1407.
[40] N.A. Lockwood, J.J. de Pablo, N.L. Abbott, Influence of surfactant tail branching and organization on the orientation of liquid crystals at Aqueous–Liquid crystal interfaces, Langmuir 21 (15) (2005) 6805–6814.
[41] F. Wang, G. Dukovic, L.E. Brus, T.F. Heinz, The optical resonances in carbon nanotubes arise from excitons, Science 308 (5723) (2005) 838–841.
[42] S.M. Bachilo, M.S. Strano, C. Kittrell, R.H. Hauge, R.E. Smalley, R.B. Weisman, Structure-assigned optical spectra of single-walled carbon nanotubes, Science 298 (5602) (2002) 2361–2366.
[43] S. Reich, C. Thomsen, P. Ordejón, Electronic band structure of isolated and bundled carbon nanotubes, Phys. Rev. B 65 (15) (2002) 155411.
[44] F. Wang, M.Y. Sfeir, L. Huang, X.M.H. Huang, Y. Wu, J. Kim, et al., Interactions between individual carbon nanotubes studied by Rayleigh scattering spectroscopy, Phys. Rev. Lett. 96 (16) (2006) 167401.
[45] J. Sim, H. Oh, E. Koo, S.-Y. Ju, Effect of tight flavin mononucleotide wrapping and its binding affinity on carbon nanotube covalent reactivities, Phys. Chem. Chem. Phys. 15 (44) (2013) 19169–19179.
[46] L. Stryer, Biochemistry, fourth ed., W.H. Freeman & Company, New York, 1995.
[47] S. Niyogi, S. Boukhalfa, S.B. Chikkannanavar, T.J. McDonald, M.J. Heben, S.K. Doorn, Selective aggregation of single-walled carbon nanotubes via salt addition, J. Am. Chem. Soc. 129 (7) (2007) 1898–1899.
[48] R.D.V. Vold, J. Marjorie, Colloid and Interface Chemistry, Addison-Wesley, 1983.
[49] A. Patist, B.K. Jha, S.-G. Oh, D.O. Shah, Importance of micellar relaxation time on detergent properties, J. Surfactants Deterg. 2 (3) (1999) 317–324.
[50] A. Patist, S.G. Oh, R. Leung, D.O. Shah, Kinetics of micellization: its significance to technological processes, Colloids Surf. A Physicochem. Eng. Asp 176 (1) (2001) 3–16.
[51] X. Wei, T. Tanaka, T. Hirakawa, Y. Yomogida, H. Kataura, Determination of enantiomeric purity of single-wall carbon nanotubes using flavin mononucleotide, J. Am. Chem. Soc. 139 (45) (2017) 16068–16071.
[52] D. Roxbury, X. Tu, M. Zheng, A. Jagota, Recognition ability of DNA for carbon nanotubes correlates with their binding affinity, Langmuir 27 (13) (2011) 8282–8293.
[53] L. Cognet, D.A. Tsyboulski, J.-D.R. Rocha, C.D. Doyle, J.M. Tour, R.B. Weisman, Stepwise quenching of exciton fluorescence in carbon nanotubes by single-molecule reactions, Science 316 (5830) (2007) 1465–1468.
[54] Y. Moroi, Micelles: Theoretical and Applied Aspects, Springer Science & Business Media, 1992.
[55] J.N. Rao, Y.E. Kim, L.S. Park, T.S. Ulmer, Effect of pseudorepeat rearrangement on α-synuclein misfolding, vesicle binding, and micelle binding, J. Mol. Biol. 390 (3) (2009) 516–529.
[56] A.V. Kabanov, I.R. Nazarova, I.V. Astafieva, E.V. Batrakova, V.Y. Alakhov, A.A. Yaroslavov, et al., Micelle formation and solubilization of fluorescent probes in poly(oxyethylene-b-oxypropylene-b-oxyethylene) solutions, Macromolecules 28 (7) (1995) 2303–2314.
[57] S.K. Hait, P.R. Majhi, A. Blume, S.P. Moulik, A critical assessment of micellization of sodium dodecyl benzene sulfonate (SDBS) and its interaction with poly(vinyl pyrrolidone) and hydrophobically modified polymers, JR 400 and LM 200, J. Phys. Chem. B 107 (15) (2003) 3650–3658.
[58] B.L. Bales, L. Messina, A. Vidal, M. Peric, O.R. Nascimento, Precision relative aggregation number determinations of SDS micelles using a spin probe. A

model of micelle surface hydration, J. Phys. Chem. B 102 (50) (1998) 10347–10358.
[59] L. Hao, R. Lu, D.G. Leaist, P.R. Poulin, Aggregation number of aqueous sodium cholate micelles from mutual diffusion measurements, J. Solut. Chem. 26 (2) (1997) 113–125.
[60] A. Heredia, M.J. Bukovac, Interaction between 2-(1-naphthyl)acetic acid and micelles of nonionic surfactants in aqueous solution, J. Agric. Food Chem. 40 (11) (1992) 2290–2293.
[61] F. Li, G.-Z. Li, J.-B. Chen, Synergism in mixed zwitterionic–anionic surfactant solutions and the aggregation numbers of the mixed micelles, Colloids Surf. A Physicochem. Eng. Asp 145 (1) (1998) 167–174.
[62] S.A. Moore, A.A. Harris, R.M. Palepu, Spectroscopic investigations on the binding of ammonium salt of 8-anilino-1-naphthalene sulfonic acid with non-ionic surfactant micelles in aqueous media, Fluid Phase Equil. 251 (2) (2007) 110–113.
[63] R.M.F. Fernandes, B. Abreu, B. Claro, M. Buzaglo, O. Regev, I. Furó, et al., Dispersing carbon nanotubes with ionic surfactants under controlled conditions: comparisons and insight, Langmuir 31 (40) (2015) 10955–10965.
[64] M.S. Strano, C.B. Huffman, V.C. Moore, M.J. O'Connell, E.H. Haroz, J. Hubbard, et al., Reversible, band-gap-selective protonation of single-walled carbon nanotubes in solution, J. Phys. Chem. B 107 (29) (2003) 6979–6985.
[65] G. Dukovic, B.E. White, Z. Zhou, F. Wang, S. Jockusch, M.L. Steigerwald, et al., Reversible surface oxidation and efficient luminescence quenching in semiconductor single-wall carbon nanotubes, J. Am. Chem. Soc. 126 (46) (2004) 15269–15276.
[66] O. Matarredona, H. Rhoads, Z. Li, J.H. Harwell, L. Balzano, D.E. Resasco, Dispersion of single-walled carbon nanotubes in aqueous solutions of the anionic surfactant NaDDBS, J. Phys. Chem. B 107 (48) (2003) 13357–13367.
[67] E.J. Wanless, W.A. Ducker, Organization of sodium dodecyl sulfate at the Graphite–Solution interface, J. Phys. Chem. 100 (8) (1996) 3207–3214.
[68] A.J. Hilmer, T.P. McNicholas, S. Lin, J. Zhang, Q.H. Wang, J.D. Mendenhall, et al., Role of adsorbed surfactant in the reaction of aryl diazonium salts with single-walled carbon nanotubes, Langmuir 28 (2) (2012) 1309–1321.
[69] P. Angelikopoulos, A. Gromov, A. Leen, O. Nerushev, H. Bock, E.E.B. Campbell, Dispersing individual single-wall carbon nanotubes in aqueous surfactant solutions below the cmc, J. Phys. Chem. C 114 (1) (2010) 2–9.
[70] M.F. Islam, E. Rojas, D.M. Bergey, A.T. Johnson, A.G. Yodh, High weight fraction surfactant solubilization of single-wall carbon nanotubes in water, Nano Lett. 3 (2) (2003) 269–273.
[71] H. Wang, Dispersing carbon nanotubes using surfactants, Curr. Opin. Colloid Interface Sci. 14 (5) (2009) 364–371.
[72] F. Palazzesi, M. Calvaresi, F. Zerbetto, A molecular dynamics investigation of structure and dynamics of SDS and SDBS micelles, Soft Matter 7 (19) (2011) 9148–9156.
[73] L.M. Bronstein, S. Dixit, J. Tomaszewski, B. Stein, D.I. Svergun, P.V. Konarev, et al., Hybrid polymer particles with a protective Shell: synthesis, structure, and templating, Chem. Mater. 18 (9) (2006) 2418–2430.
[74] N.A. Mazer, M.C. Carey, R.F. Kwasnick, G.B. Benedek, Quasielastic light scattering studies of aqueous biliary lipid systems. Size, shape, and thermodynamics of bile salt micelles, Biochemistry 18 (14) (1979) 3064–3075.
[75] H.H. Paradies, Shape and size of a nonionic surfactant micelle. Triton X-100 in aqueous solution, J. Phys. Chem. 84 (6) (1980) 599–607.

Supporting Information for

Scaling of Binding Affinities and Cooperativities of Surfactants on Carbon Nanotubes

Minsuk Park[1], Junmo Park[1], Jiyun Lee[2], and Sang-Yong Ju[1,*]

[1]Department of Chemistry, and [2]Department of Chemical and Biomolecular Engineering, Yonsei University, 50 Yonsei-ro, Seodaemun-Gu, Seoul 03722, Korea

* Corresponding author Tel. +82-2-2123-5639. E-mail: syju@yonsei.ac.kr (Sang-Yong Ju)

Table of Contents **S1-2**

Figure S1. Absorption spectra of the HiPco SWNTs dispersed by various surfactants. The dispersion whose absorption value exceeds limits of this spectrometer (JASCO 770) is subjected to diluted measurement in appropriate concentration and was then multiplied by dilution factor to display absorbance to facilitate visual comparison.

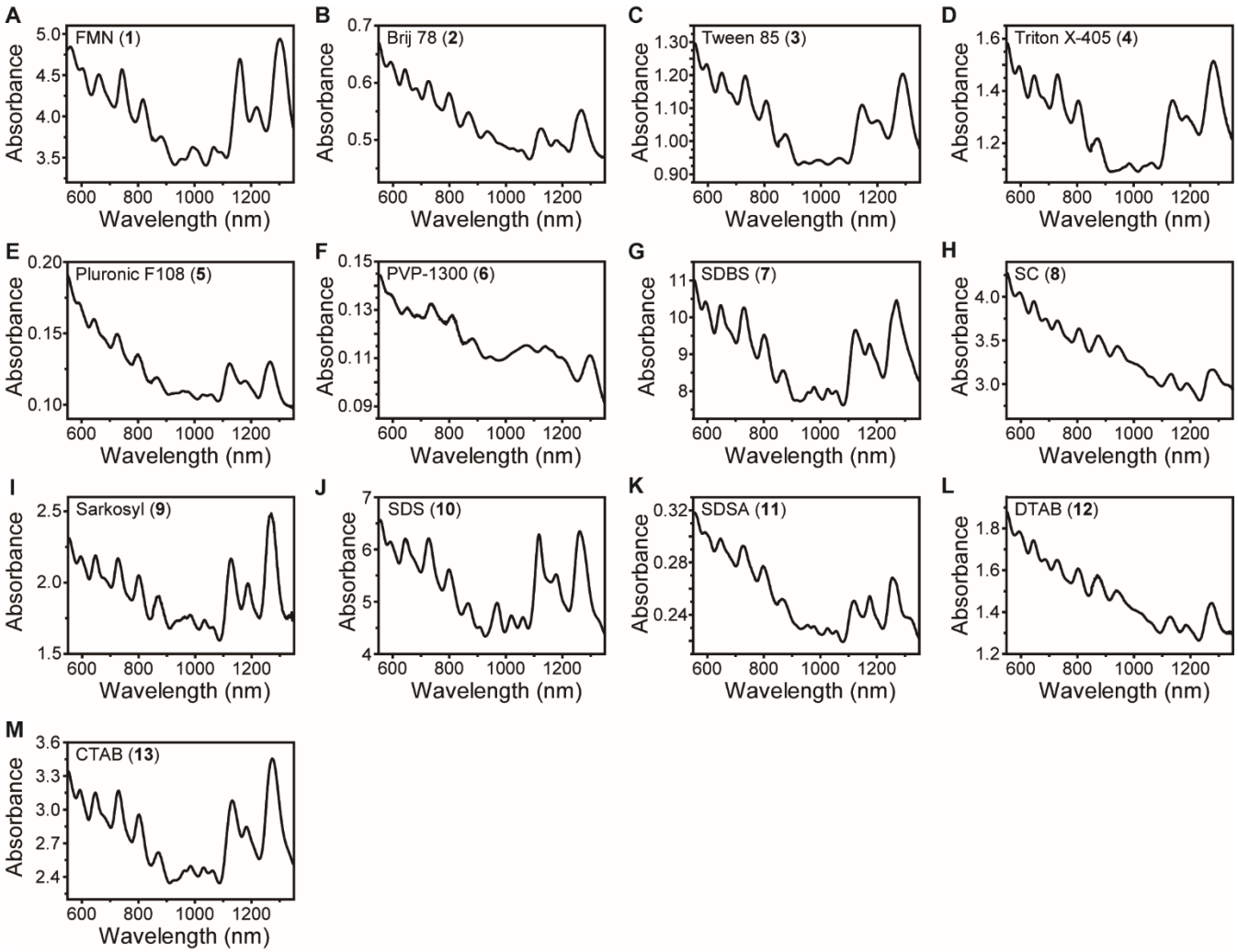

Figure S2. PLE maps of HiPco SWNTs dispersed by various surfactants except SDS-HiPco dispersion displayed as inset of Figure 2B in the main text.

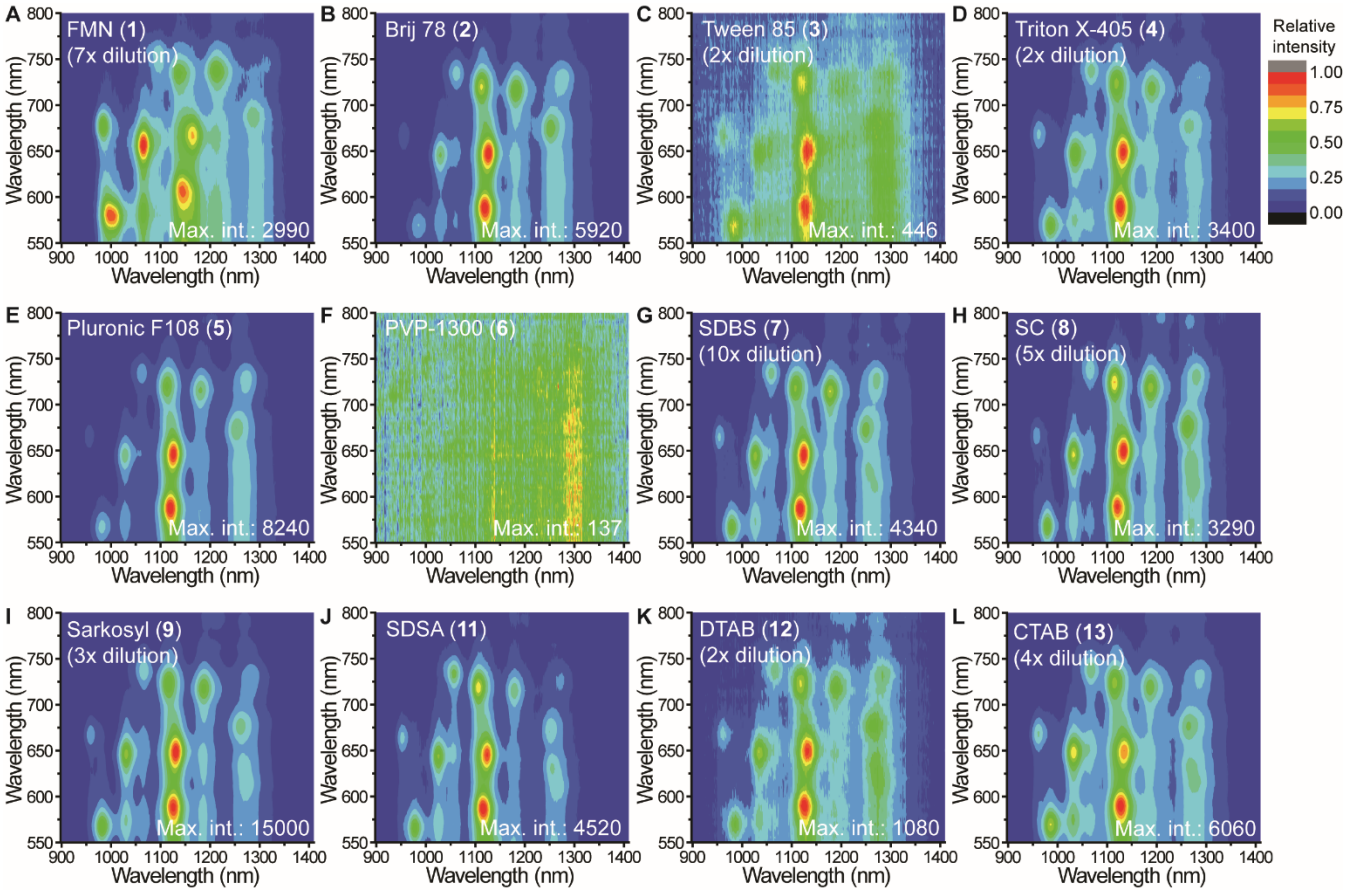

Figure S3. Comparison of the PL position shift of our results with the literature.[S1] Red and black symbols indicate a PL shift of (6,5) tube of various surfactant against that of SDS, and PL shift of (8,3) tube from the reference.[S1]

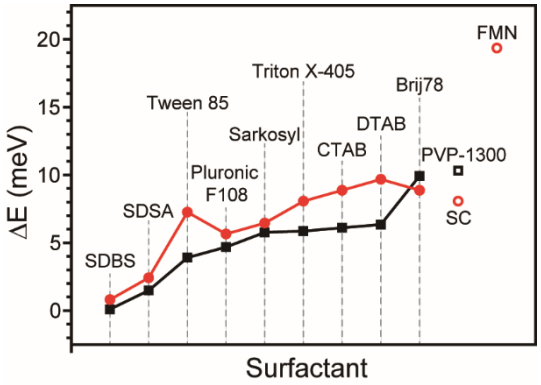

Figure S4. Time-dependent PL spectra change of FMN-SWNTs with time interval of 4 sec upon the addition of excess SDBS (i.e., 1.7 mM). (A) A series of emission spectra after the addition probed by excitation wavelength of 660 nm. The reason for having PL peak of FMN-(7,5) tube after the completion originates from the PL contribution from the occurrence of SDBS-replaced (10,2) chirality. (B) I_{PL} trajectories of FMN-(7,5) (square) and SDBS-(7,5) (circle) over time. I_{PL} trends were fitted by logarithmic equation. (C and D) The similar spectrum changes and I_{PL} trends for (8,6) tube.

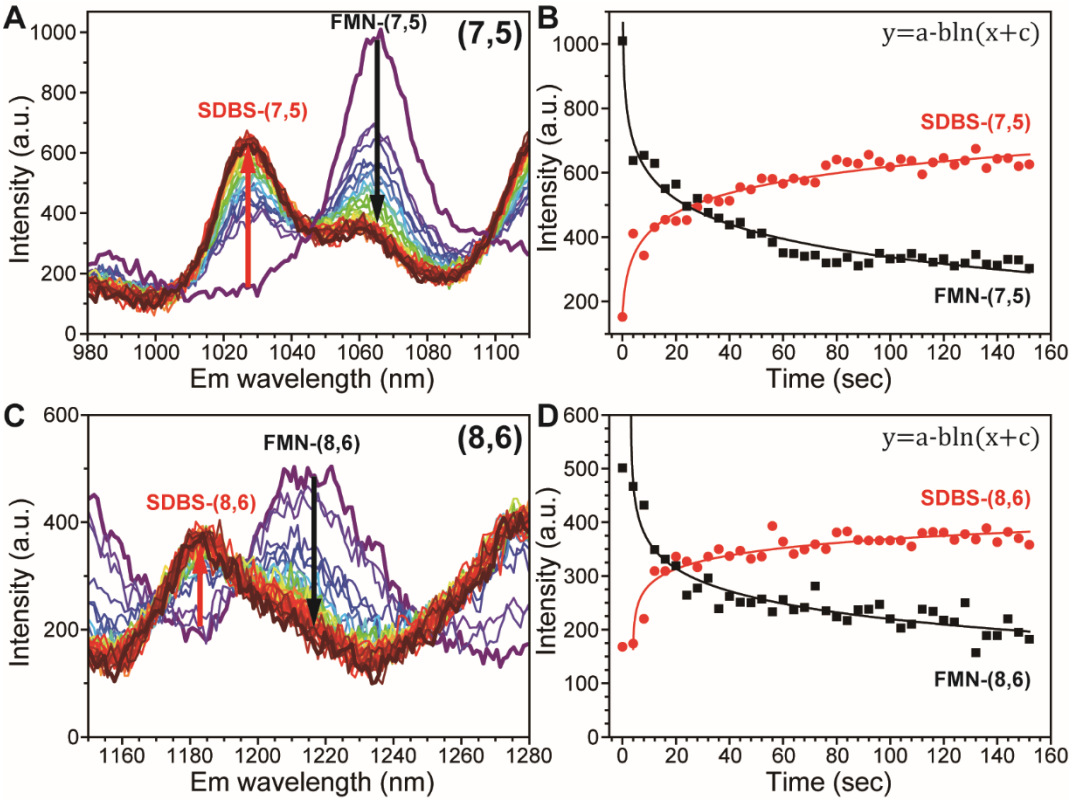

Figure S5. PLE maps after surfactant exchange on SWNT. (A) PLE map of initial dispersion with FMN (B-J) and after surfactant exchange with various surfactant.

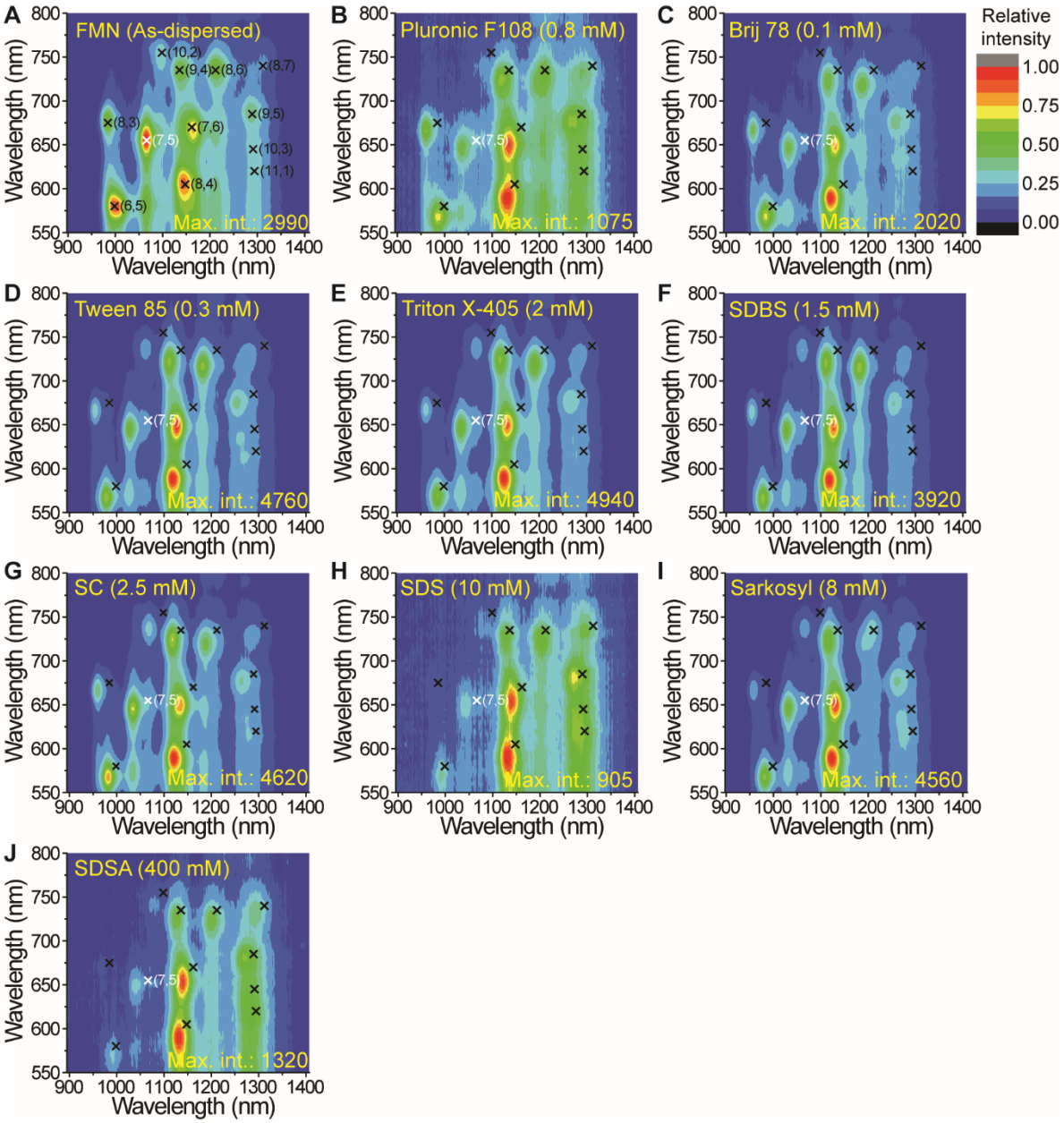

Figure S6. Chirality-dependent K_d patterns of various surfactants as a function of SWNT d_t. The linear regression of K_d value is indicated in red dotted line. Note that SDBS- and SC-suspended HiPco has *P*- and *M*-handedness which is indicated by blue and red symbols.

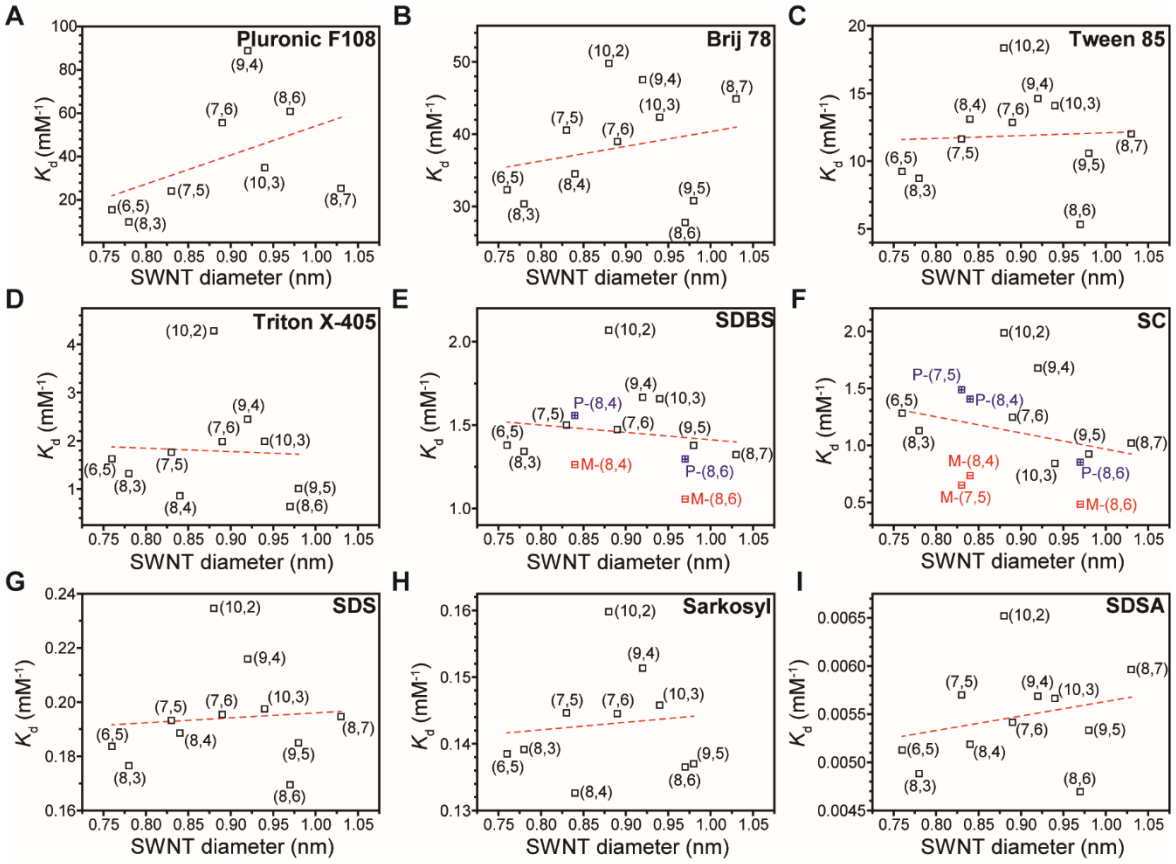

Figure S7. The corresponding full absorption spectra upon the titration of SDBS against FMN-HiPco.

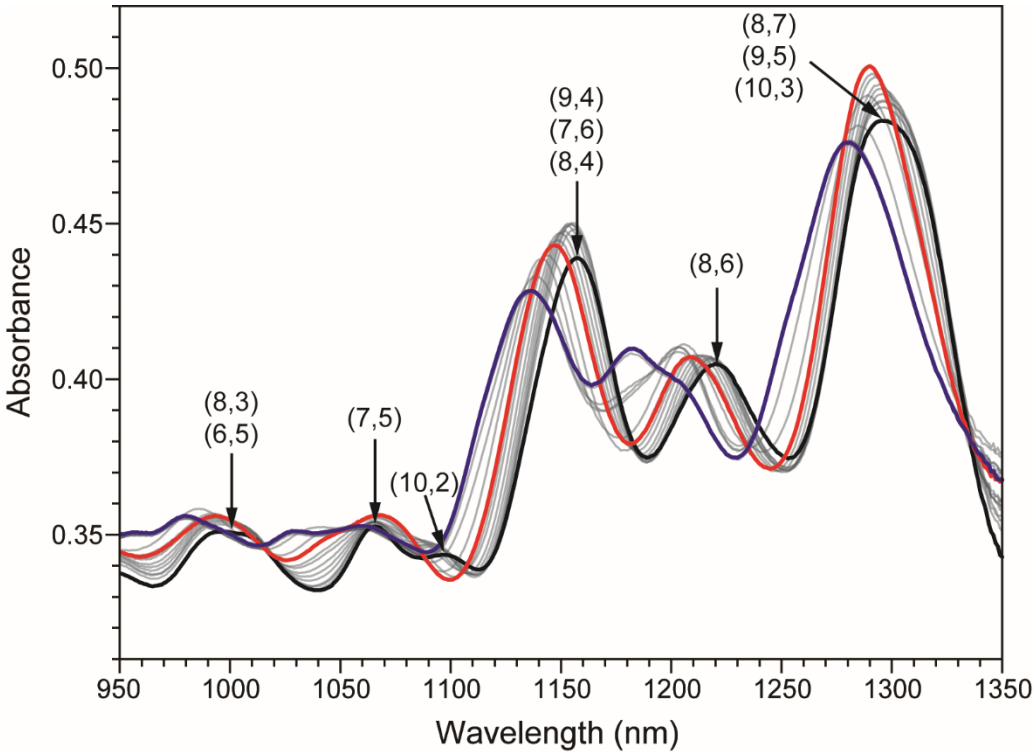

Figure S8. Histograms of SWNT chiralities after the surfactant exchange based on I_{PL}.

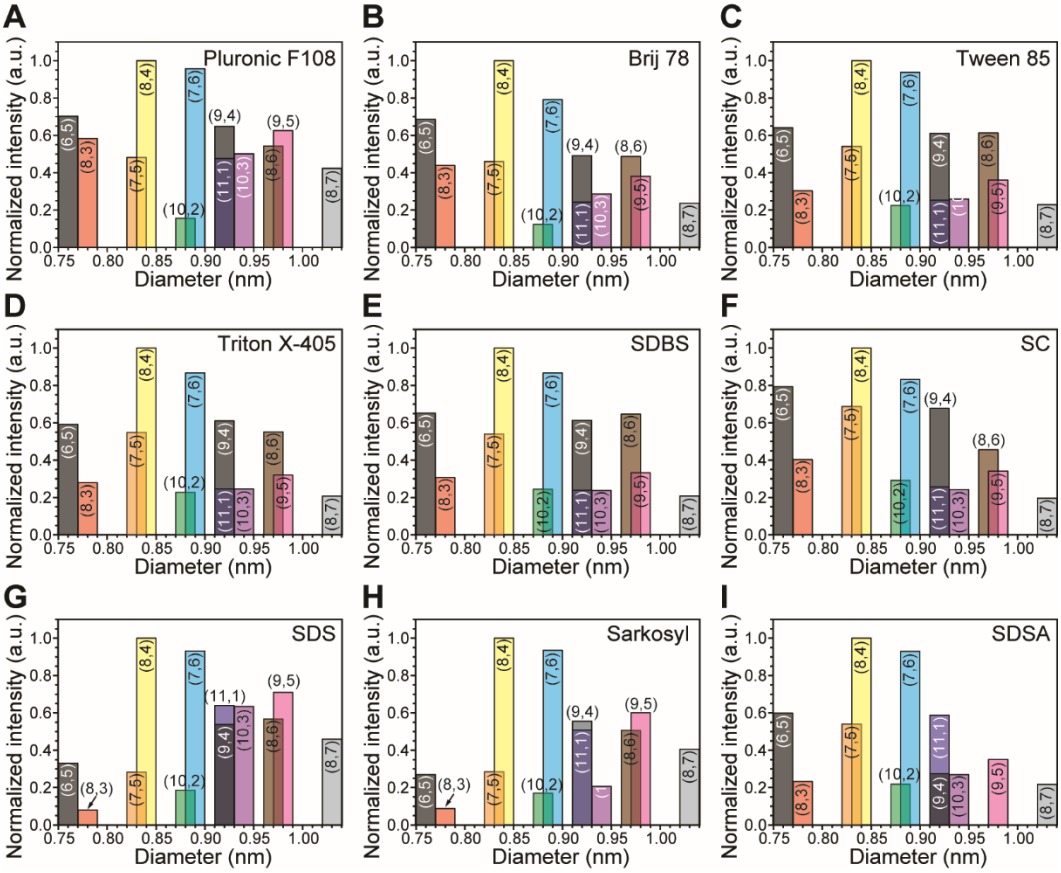

Figure S9. pH control experiments after the surfactant exchange. (A) PLE maps of before (left), after the addition of Pluronic F108 (0.2 mM, middle) which is further added with NaOH (right). The corresponding absorption spectrum (B) before (black), after the titration (0.2 mM, red), and further addition of NaOH (blue). (C-F) PL change trends after the titration and basification of various surfactants.

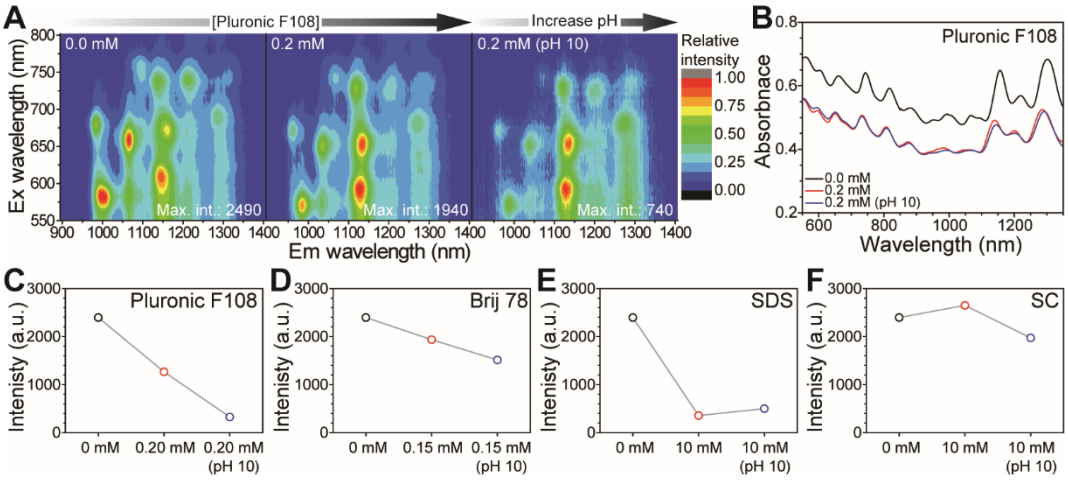

Figure S10. Relationship between K and average ΔG according to the surfactant exchange. The different symbols indicate types of surfactant and number of symbols denotes nanotube chiralities.

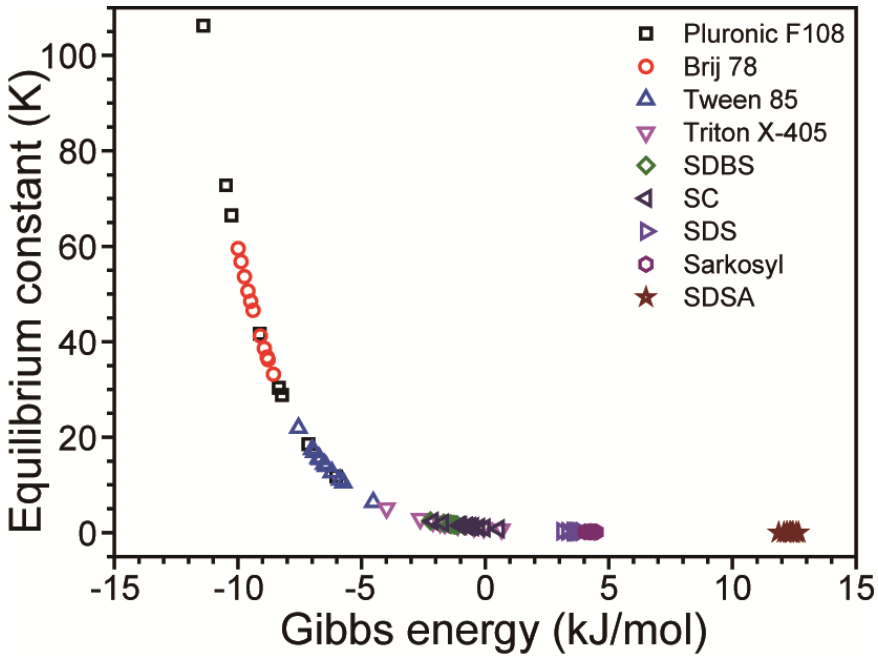

Table S1. Full description of surfactants used in this study.

No.	Chemical name	Abbreviation	Type†	Hydrophilic group‡	Hydrophobic group※	CMC (mM)	CMC Ref.	Conc. at 1 wt/v % (mM)	M.W. (g/mol)
1	Flavin mononucleotide	FMN	–	*d*-ribityl, -OP(OH)O_2^-	Isoalloxazine	-		N.A.	478.33
2	Polyoxyethylene oleyl ether	Brij 78	non	-E20	-C18	0.046	[S2]	8.35	1,151.56
3	Polyoxyethylene sorbitan trioleate	Tween 85	non	-sorbitan-E_w,-E_x,-E_y,-E_z, $w+x+y+z=20$	3×-C17	0.0125	[S3]	5.09	~1,839
4	Polyethylene glycol *tert*-octylphenyl ether	Triton X-405	non	-E40	-$(C_6H_4)C(CH_2)_2CH_2C(CH_3)_3$	0.81	[S4]	5.44	~1,967
5	PEG-PPG-PEG	Pluronic F108	non	-E_x,-E_z	-P_y-	0.51	[S5]	0.68	~14,600
6	Poly(vinylpyrrolidone)	PVP-1300	non	-pyrrolidone	Polyvinyl-	unknown		N.A.	~1,300k
7	Sodium dodecylbenzenesulfonate	SDBS	–	-SO_3^-	-C12	1.20	[S6]	28.7	348.48
8	Sodium cholate	SC	–	-COO^-	Steroid	14.0	[S4]	23.23	430.56
9	Sodium dodecanoyl sarcosine	Sarkosyl	–	-$CONHCH_2COO^-$	-C11	14.0	[S4]	34.08	293.40
10	Sodium dodecyl sulfate	SDS	–	-OSO_3^-	-C12	8.0	[S6]	34.68	288.38
11	Sodium dodecyl sulfonate	SDSA	–	-SO_3^-	-C12	12.0	[S7]	36.71	272.38
12	Dodecyltrimethylammonium bromide	DTAB	+	-$N^+(CH_3)_3$	-C12	0.0046	[S4]	N.A.	308.34
13	Cetyltrimethylammonium bromide	CTAB	+	-$N^+(CH_3)_3$	-C16	1.0	[S4]	N.A.	364.46

† –; anionic, +; cationic, non; nonionic.

‡ -En-;-$(OCH_2CH_2)_nOH$.

※ -Cn;-$(CH_2)_{n-1}CH_3$, -Pn-;-$(OCH_2C(CH_3)H)_n$-

Table S2. PLE-derived e^S_{11} and e^S_{22} positions of SWNT dispersed with various cosurfactants according to chiral SWNTs. d_t is based on C-C distance with 0.1421 nm.

Assignment			FMN			Brij 78			Tween 85			Triton X-405			Pluronic F108			SDBS		
(*n*,*m*)	d_t [nm]	Chiral Angle [°]	E^S_{11} [nm]	E^S_{22} [nm]	Relative Intensity	E^S_{11} [nm]	E^S_{22} [nm]	Relative Intensity	E^S_{11} [nm]	E^S_{22} [nm]	Relative Intensity	E^S_{11} [nm]	E^S_{22} [nm]	Relative Intensity	E^S_{11} [nm]	E^S_{22} [nm]	Relative Intensity	E^S_{11} [nm]	E^S_{22} [nm]	Relative Intensity
(6,5)	0.75	27	998	580	0.90	985	569	0.25	983	570	0.75	984	568	0.53	981	567	0.29	975	567	0.52
(8,3)	0.77	15.3	982	676	0.58	958	666	0.14	963	666	0.40	961	678	0.27	954	667	0.12	951	665	0.26
(7,5)	0.82	24.5	1065	657	1.00	1030	645	0.43	1034	647	0.54	1036	647	0.58	1028	646	0.40	1025	644	0.62
(8,4)	0.83	19.1	1146	606	0.90	1120	588	1.00	1125	590	0.97	1127	589	1.00	1120	588	1.00	1114	587	1.00
(10,2)	0.87	8.9	1097	754	0.32	1061	734	0.30	1060	737	0.42	1066	738	0.38	1062	734	0.23	1056	734	0.38
(7,6)	0.88	27.5	1166	667	0.77	1127	647	1.00	1130	651	1.00	1133	649	0.96	1127	647	0.98	1123	646	0.99
(9,4)	0.90	17.5	1137	734	0.54	1113	719	0.69	1120	726	0.71	1120	723	0.61	1113	721	0.53	1105	717	0.59
(10,3)	0.92	12.7	1291	648	0.31	1255	631	0.32	1274	630	0.52	1270	632	0.29	1259	632	0.32	1254	628	0.35
(8,6)	0.95	25.3	1211	737	0.56	1182	716	0.58	1196	718	0.44	1192	718	0.46	1181	716	0.43	1175	715	0.67
(9,5)	0.96	20.6	1285	688	0.40	1252	675	0.49	1280	681	0.59	1267	677	0.36	1254	673	0.42	1247	673	0.46
(8,7)	1.01	27.8	1308	740	0.18	1277	728	0.31	1288	727	0.41	1286	732	0.24	1272	726	0.31	1270	727	0.37

Assignment			SC			Sarkosyl			SDS			SDSA			DTAB			CTAB		
(*n*,*m*)	d_t [nm]	Chiral Angle [°]	E^S_{11} [nm]	E^S_{22} [nm]	Relative Intensity	E^S_{11} [nm]	E^S_{22} [nm]	Relative Intensity	E^S_{11} [nm]	E^S_{22} [nm]	Relative Intensity	E^S_{11} [nm]	E^S_{22} [nm]	Relative Intensity	E^S_{11} [nm]	E^S_{22} [nm]	Relative Intensity	E^S_{11} [nm]	E^S_{22} [nm]	Relative Intensity
(6,5)	0.75	27	984	568	0.83	982	568	0.58	974	566	1.00	977	566	0.54	986	570	0.52	985	570	0.68
(8,3)	0.77	15.3	957	666	0.42	959	667	0.22	956	668	0.35	954	664	0.27	961	669	0.26	962	668	0.34
(7,5)	0.82	24.5	1043	646	0.65	1031	646	0.63	1028	646	0.58	1025	644	0.95	1035	648	0.67	1032	648	0.74
(8,4)	0.83	19.1	1123	589	0.86	1126	589	0.96	1119	588	0.87	1116	587	1.00	1124	590	1.00	1129	590	1.00
(10,2)	0.87	8.9	1059	738	0.31	1066	737	0.33	1063	737	0.37	1057	734	0.45	1067	737	0.40	1069	738	0.40
(7,6)	0.88	27.5	1137	650	1.00	1132	648	1.00	1118	644	0.88	1125	645	0.95	1131	649	0.95	1135	649	0.84
(9,4)	0.90	17.5	1119	725	0.74	1116	723	0.58	1112	722	0.51	1108	718	0.73	1118	723	0.68	1116	724	0.62
(10,3)	0.92	12.7	1272	632	0.26	1265	632	0.29	1262	632	0.28	1256	630	0.35	1268	645	0.43	1266	632	0.36
(8,6)	0.95	25.3	1188	719	0.31	1188	717	0.53	1183	717	0.36	1179	715	0.39	1190	717	0.53	1186	718	0.48
(9,5)	0.96	20.6	1261	676	0.36	1261	676	0.38	1262	676	0.33	1250	672	0.32	1265	677	0.53	1265	677	0.43
(8,7)	1.01	27.8	1280	730	0.19	1282	730	0.24	1286	731	0.22	1273	725	0.17	1283	731	0.43	1287	729	0.28

Table S3. K_a and γ of the FMN-HiPco against various surfactants along with standard deviation (STD). Asterisk indicates that these larger values originate from the uncertainty of fitting two abrupt data points without any intermediate, which were omitted for the calculation of the average value.

Surfactant / Assignment	Brij 78 (2)				Tween 85 (3)				Triton X-405 (4)				Pluronic F108 (5)				SDBS (7)			
	K_a	STD	γ	STD	K_a	STD	γ	STD	K_a	STD	γ	STD	K_a	STD	γ	STD	K_a	STD	γ	STD
(6,5)	0.031	0.0004	9.56	1.1621	0.11	0.0009	6.97	0.3547	0.61	0.0148	7.72	1.3915	0.064	0.0020	4.77	0.4404	0.73	0.0024	31.28	2.5873
(8,3)	0.033	0.0002	26.67	2.1419	0.11	0.0011	12.46	1.2996	0.76	0.0060	20.08	2.2412	0.102	0.0021	4.55	0.4482	0.74	0.0028	56.40	19.6117
(7,5)	0.025	0.0004	8.39	0.9270	0.09	0.0013	7.17	0.6474	0.57	0.0216	14.02	5.8275	0.041	0.0005	4.84	0.2006	0.67	0.0026	36.21	3.8055
(8,4)	0.029	0.0008	7.45	1.2183	0.08	0.0013	8.70	1.2091	1.17	0.0267	39.21	24.0098					0.72	0.0072	26.30	6.8823
(10,2)	0.020	6.4295*	75.64*	-	0.05	0.0019	14.34	4.9982	0.23	0.0143	15.86	5.7866	0.004	0.0004	2.40	0.3717	0.48	0.0515	9.90	11.0634
(7,6)	0.026	0.0001	19.12	2.3877	0.08	0.0008	8.94	0.6748	0.50	0.0113	10.00	2.2408	0.018	0.0004	4.01	0.2954	0.68	0.0024	22.26	1.4734
(9,4)	0.021	0.0003	10.07	1.3438	0.07	0.0010	19.95	6.1633	0.41		90.75*		0.011	0.0003	5.41	0.6520	0.60		347.55*	
(10,3)	0.024	0.0008	8.44	1.9356	0.07	0.0024	5.71	1.0449	0.50		104.85*	-	0.029	0.0027	3.50	0.8289	0.60	0.0982	5.08	7.8301
(8,6)	0.036	0.0004	11.17	1.2609	0.19	0.0044	11.23	2.8134	1.57	0.0108	22.10	3.5079	0.016	0.0054	0.93	0.2123	0.86	0.0079	46.16	15.1648
(9,5)	0.032	0.0006	24.07	5.1657	0.09	0.0122	4.17	2.2806	0.99	0.0617	6.83	1.0708					0.73	0.0071	55.24	14.8485
(8,7)	0.022	0.0016	7.77	3.2439	0.08	0.0085	3.60	1.3361					0.039	0.0080	1.34	0.4059	0.76	0.0160	47.60	58.1625
Average	0.027	0.0006	13.27	2.0787	0.09	0.0033	9.38	2.0747	0.73	0.0209	16.98	5.7595	0.036	0.0024	3.53	0.4284	0.68	0.0198	33.64	14.1429

Surfactant / Assignment	SC (8)				Sarkosyl (9)				SDS (10)				SDSA (11)			
	K_a	STD	γ	STD	K_a	STD	γ	STD	K_a	STD	γ	STD	K_a	STD	γ	STD
(6,5)	0.78	0.0033	11.26	0.4541	7.22	0.0100	115.11	16.5300	5.44	0.0425	19.39	2.7331	195.01	2.4478	15.00	2.4533
(8,3)	0.89	0.0036	11.37	0.4631	7.19	0.0076	116.82	12.9344	5.66	0.0548	25.79	5.7186	204.78	3.4123	36.77	22.4294
(7,5)	1.10	0.0139	10.46	1.3295	6.91	0.0081	240.41	88.8085	5.17	0.0438	21.89	3.8708	175.44	2.0302	15.12	2.5325
(8,4)	1.04	0.0089	25.70	7.9475	7.54	0.0071	214.96	29.7422	5.30	0.1153	8.96	1.7343	192.77	3.3437	9.60	1.4104
(10,2)	0.50	0.0057	13.59	2.3979	6.26	0.0172	88.34	20.7031	4.26	0.0624	24.46	5.5323	153.37	1.7164	19.91	5.1944
(7,6)	0.80	0.0085	7.27	0.5074	6.92	0.0060	116.72	8.3304	5.12	0.0313	28.02	4.5607	184.66	1.8441	21.59	3.1623
(9,4)	0.60	0.0077	18.34	5.0739	6.61		1286.30*		4.63	0.0446	32.44	7.9141	175.87	3.1812	16.72	5.1948
(10,3)	1.19	0.1192	7.09	4.5754	6.86		6742.92*		5.06	0.0469	34.76	11.1781	176.56	-	148.51*	-
(8,6)	1.62	0.0323	16.60	5.7157	7.33	0.0210	103.10	27.9126	5.90	0.0673	9.93	1.1056	213.00	3.4085	8.65	1.0793
(9,5)	1.08	0.0092	26.10	5.0905	7.30	0.0371	90.22	39.7202	5.41	0.0551	18.33	3.3531	187.57	4.1599	11.95	2.7165
(8,7)	0.98	0.0157	55.33	-					5.14	0.0845	92.00*	-	167.71	7.9178	9.35	3.5240
Average	0.96	0.0207	18.46	3.3555	7.01	0.0143	135.71	30.5852	5.19	0.0589	22.40	4.7701	184.25	3.3462	16.47	4.9697

Table S4. K_d values of the various surfactants according to SWNT chiralities. Asterisk indicates that these larger values originate from the uncertainty of fitting two abrupt data points without any intermediate and was omitted for the calculation of the average value.

SWNT chirality	K_d (mM^{-1})								
	Pluronic F108 (5)	Brij 78 (2)	Tween 85 (3)	Triton X-405 (4)	SDBS (7)	SC (8)	SDS (10)	Sarkosyl (9)	SDSA (11)
(6,5)	15.52	32.29	9.24	1.627	1.379	1.281	0.184	0.139	0.00513
(8,3)	9.84	30.34	8.74	1.319	1.343	1.128	0.177	0.139	0.00488
(7,5)	24.16	40.55	11.64	1.764	1.500	1.069	0.193	0.145	0.00570
(8,4)	--	34.50	13.11	0.858	1.410	1.070	0.189	0.133	0.00519
(10,2)	225.23*	49.80	18.36	4.283	2.068	1.985	0.235	0.160	0.00652
(7,6)	55.62	38.97	12.86	1.987	1.473	1.247	0.195	0.145	0.00542
(9,4)	88.89	47.51	14.62	2.449	1.666	1.676	0.216	0.151	0.00569
(10,3)	34.88	42.36	14.11	1.990	1.658	0.842	0.198	0.146	0.00566
(8,6)	60.90	27.77	5.34	0.638	1.177	0.668	0.170	0.137	0.00469
(9,5)	--	30.79	10.59	1.008	1.378	0.923	0.185	0.137	0.00533
(8,7)	25.39	44.86	12.02	--	1.322	1.020	0.195	--	0.00596
Average	39.40	38.16	11.88	1.792	1.489	1.173	0.194	0.143	0.00547

Cited references

[S1] V.C. Moore, M.S. Strano, E.H. Haroz, R.H. Hauge, R.E. Smalley, J. Schmidt, et al., Individually Suspended Single-Walled Carbon Nanotubes in Various Surfactants, Nano Lett. 3(10) (2003) 1379-1382.

[S2] C. Klammt, D. Schwarz, K. Fendler, W. Haase, V. Dötsch, F. Bernhard, Evaluation of detergents for the soluble expression of α-helical and β-barrel-type integral membrane proteins by a preparative scale individual cell-free expression system, FEBS J. 272(23) (2005) 6024-6038.

[S3] L.S.C. Wan, P.F.S. Lee, CMC of polysorbates, J. Pharm. Sci. 63(1) (1974) 136-137.

[S4] T. Tanaka, Y. Urabe, D. Nishide, H. Kataura, Discovery of Surfactants for Metal/Semiconductor Separation of Single-Wall Carbon Nanotubes via High-Throughput Screening, J. Am. Chem. Soc. 133(44) (2011) 17610-17613.

[S5] J.R. Lopes, W. Loh, Investigation of Self-Assembly and Micelle Polarity for a Wide Range of Ethylene Oxide−Propylene Oxide−Ethylene Oxide Block Copolymers in Water, Langmuir 14(4) (1998) 750-756.

[S6] Y. Shi, H.Q. Luo, N.B. Li, Determination of the critical premicelle concentration, first critical micelle concentration and second critical micelle concentration of surfactants by resonance Rayleigh scattering method without any probe, Spectrochim. Acta A 78(5) (2011) 1403-1407.

[S7] N.A. Lockwood, J.J. de Pablo, N.L. Abbott, Influence of Surfactant Tail Branching and Organization on the Orientation of Liquid Crystals at Aqueous−Liquid Crystal Interfaces, Langmuir 21(15) (2005) 6805-6814.